RSC Advances

REVIEW

View Article Online
View Journal | View Issue

Cite this: *RSC Adv.*, 2021, **11**, 3020

Carbon nanotube materials for electrocardiography

Anna Kolanowska,[a] Artur P. Herman,[ab] Rafał G. Jędrysiak[a] and Sławomir Boncel[*a]

Received 12th October 2020
Accepted 7th January 2021

DOI: 10.1039/d0ra08679g

rsc.li/rsc-advances

Carbon nanotubes (CNTs) as 1D nanomaterials of excellent physicochemical characteristics bring hope to compete and eventually conquer traditional solutions in electrocardiography – one of the most powerful and non-invasive diagnostic tools in cardiac disorders. Our review tracks (from 2008) the development of CNTs as critical components in the systems where CNTs serve mainly as electroconductive fillers hence enable recording electrocardiographs (ECG). The characteristics of the CNT-based ECG systems – mainly to-skin electrodes and in a few cases wiring – covers their electrical and mechanical performance (adhesivity, flexibility, elasticity) and qualitative biocompatibility. By comprehensive analysis of the state-of-art in this field, we intend to indicate the most important challenges for the CNT (and other) materials to be applied in scale-up solution for electrocardiography in the near future.

1. Introduction

The modern story of carbon nanotubes (CNTs) began with 'Helical microtubules of graphitic carbon' – the ground-breaking paper by Iijima.[1] Due to their inherent and unusual combination of excellent physicochemical properties, CNTs have rapidly gained the scientific community's attention. As novel high-performance characteristics of CNTs have been revealed, their applications were only a matter of time. Nowadays produced in a thousand-tonne scale yearly,[2] CNTs firmly became 'the star of nanotechnology' with numerous applications brought to every-day life – with a few yet waiting in the queue (Fig. 1A). Those areas range from microelectronics (field-effect transistors,[3,4] microprocessors[5]), stealth technology,[6] energy storage,[7,8] heat transfer,[9] composite materials,[10,11] functional coatings[12] and films[13,14] to, key here, biotechnology and medicine (drug delivery,[15–17] biosensors[18,19]). The list is incomplete while the indicated areas naturally intertwine and cross-inspire.[20–22] But medicine is the field promised to mostly benefit from the CNT extraordinary characteristics with the risk allocated only to matrix-free or non-functionalized (pristine) nanotubes of high aspect ratio.[23] Within contemporary medicine, diagnostics and 'theranostics' (therapy + diagnostics)

[a]*Department of Organic Chemistry, Bioorganic Chemistry and Biotechnology, Faculty of Chemistry, Silesian University of Technology, NanoCarbon Group, Bolesława Krzywoustego 4, 44-100 Gliwice, Poland. E-mail: slawomir.boncel@polsl.pl; Fax: +48 32 237 20 94; Tel: +48 32 237 12 72*

[b]*Department of Semiconductor Materials Engineering, Faculty of Fundamental Problems of Technology, Wrocław University of Science and Technology, Wybrzeże Wyspiańskiego 27, 50-370 Wrocław, Poland*

Anna Kolanowska obtained a PhD degree in chemistry from the Silesian University of Technology in 2020 under the guidance of Prof. Boncel. In 2020 she joined Prof. Przemysław Data's group at the Silesian University of Technology. Her research interests focus on the synthesis, surface engineering and applications of carbon nanomaterials (carbon nanotubes, quantum dots, graphene) and organic electronics in various fields form medicine to civil and military engineering.

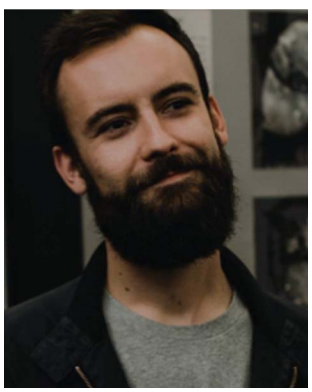

Artur P. Herman obtained a PhD degree in chemistry from Silesian University of Technology in 2017 under the guidance of Prof. Boncel. In 2018 he joined Prof. Robert Kudrawiec's group at the Wroclaw University of Science and Technology. His research interests include inter alia heterostructures based on low-dimensional nanomaterials, interfacial phenomena, solar cells, photoelectrochemistry, modulation spectroscopy and charge-carrier kinetics in semiconductors.

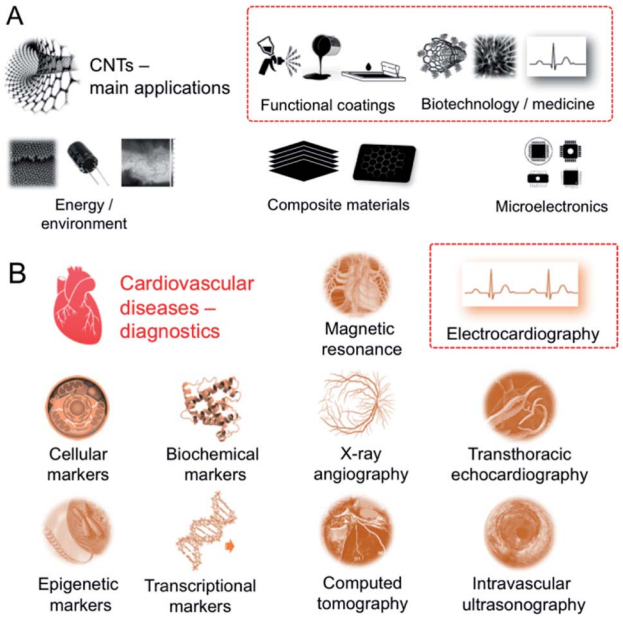

Fig. 1 (A) Main areas of CNT current applications; (B) diagnostic tools for cardiovascular diseases.

represent the areas of the greatest promise of CNT applications since the CNT hybrid tools can be tailored to specific requirements practically at the nanoscale. One of the main challenges here is prophylaxis and treatment of civilization disorders – with the cardiovascular diseases as the most lethal ones.[24] Globally, nearly one in every three deaths (31%) can be assigned thereto. Actually, at the time-scale of reading these sentences, a hundred of people in the world have just died of the cardiovascular disease. Hence, the rationale behind demand for added-value scientific and technological solutions is clear and natural. And although the main factors elevating the risk of cardiovascular diseases lie practically under the given person's authority (smoking cigarettes, inadequate diet, insufficient physical activity and stress – leading to high blood concentration of low-density lipoprotein cholesterol, elevated blood pressure, or overweight) and/or have a possible other (co) genesis (with type 2 diabetes being the most frequent co-existing and risk-elevating), prophylaxis and early diagnosis – with accessible and convenient tools – remain beneficial both for the patient and the healthcare systems.[25] The demand is also critical since perceptible symptoms of cardiovascular diseases are rather late, qualitative and in fact emergency-calling. There is a clear world-wide call for scalable and reliable high throughput diagnostic tools.

Electrocardiography (ECG) – being both very convenient and informative – lies therefore in the heart of heart monitoring[26] (Fig. 1B). Among others, non- or low-invasive techniques: interview focused on personal/family medical history, blood tests toward specific markers (cellular, biochemical, epigenetic, transcriptional), chest X-ray, echocardiography, computerized tomography (CT), magnetic resonance imaging (MRI), and angiography to invasive, *i.e.* cardiac catheterization, ECG is simply the first-choice technique. It is in fact the most expedient, versatile and powerful technique being in the same time inexpensive, *ergo* broadly accessible. Development of ECG requires complex and frequently hierarchical materials of enhanced characteristics – from economic to mechanical to electrical – toward reliable performance in the all-in-one (multitask) and compatible devices.[27]

The motivation for writing this review is twofold. Firstly, the review concerns one of the greatest promises of CNT applications, *i.e.* contemporary cardiologic electrodiagnostics. This

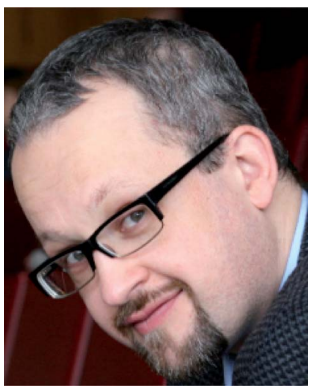

Rafał G. Jędrysiak obtained a PhD degree in chemistry (2008) from the Silesian University of Technology under the Prof. Suwiński's supervision. In 2014 he worked as a scientific consultant in Department of Materials Science and Metallurgy, University of Cambridge, UK. He was a post-doc in 2016 in Intelligent Polymer Research Institute at University of Wollongong, Australia. His current research interest concerns industrial applications of carbon nanomaterials and composites.

Slawomir Boncel, head of NanoCarbon Group, completed PhD in organic chemistry (2009) and DSc (habilitation, 2015) in nanocarbon chemistry at the Silesian University of Technology. In 2013 he received a 15 month post-doc scholarship in the Department of Materials Science at University of Cambridge, UK, financed by Foundation for Polish Science to perform research studies on magnetically targeted carbon nanotubes (CNTs) as drug delivery systems. His research interests include synthesis, physicochemistry and applications of carbon nanoallotropes; specifically: high-performance CNT nanocomposites and hybrid materials, electroconductive coatings, stealth technology, drug delivery systems, and heat transfer nanofluids. He is an author of >70 publications (Hirsch index 19, ~1200 citations) and currently a lecturer in his Alma Mater.

derives from the fact that electrical properties of CNT-based materials/devices can be tailored practically at the nanoscale. And CNTs – wondrous components of complex systems – promise to conquer many problems related to metal or liquid electrolytes and the corresponding interfaces. Secondly, in fighting cardiac disorders – the most lethal and increasingly threatening civilization diseases – prophylaxis and early detection are the most powerful tools. Here, long-term ECG, including remote monitoring, becomes a standard diagnostic means, particularly for aging societies. Moreover, the existing solutions frequently suffer from inconvenience, limited reproducibility or complex manufacturing, while CNTs – with their combination of unique properties and processability – might create innovative solutions for ECG, but the most pressing problems and challenges must be clearly identified. Hence, getting acquainted with our review will be a condition of being updated about the progress in applications of carbon nanotubes as functional/textronic coatings while the readers will experience cross-inspiring analysis as the subject of the review is multidisciplinary.

In summary, with this review, facing all the challenges, we aim to highlight the recent advances in the field of biomedical CNT-based sensors, including textronics as the main one. One could claim without exaggeration that ECG sensors using CNTs as the electroactive component – with all their other superior parameters – have dominated the contemporary approaches. And having comprehensively analysed the so-far achievements, we attempt to indicate the general outcomes and formulate the future perspectives of the CNT-based ECG eventually.

2. Fundamentals of electrocardiography – overview and requirements for novel materials

While design of novel of added-value ECG materials firstly requires comprehensive understanding of the nature of heart functioning, the reader is sent to the relevant comprehensive sources.[28,29] Nevertheless, some key points should be recalled. Generally, ECG monitors state of the heart by recording its electrical signals. More precisely, it acquires electrical impulses generated by polarization and depolarization of the cardiac tissue while the graphical representation of those complex phenomena is the *quasi*-periodic function in time.[30] The composite data allows measuring rate and orderliness of the heartbeats directly and, indirectly, determining size and position of the chambers including any type of the heart failures or irregularities at large. Ion flow across the heart cell membranes induces the electrical current with the main electrolytes Na^+, K^+, Ca^{2+} and Cl^-. The flow of ions could be observed as positive or negative waveform on the electrocardiogram called P-, QRS- and T-waves in the appropriate time-scale (Fig. 2A).[31]

The first P-peak is connected to the atrial depolarization and the spread of electrical impulse throughout the right and left atria. The subsequent QRS-complex wave is related to the spread of electrical impulse through the ventricles. Both features represent depolarization process when the stimulus –

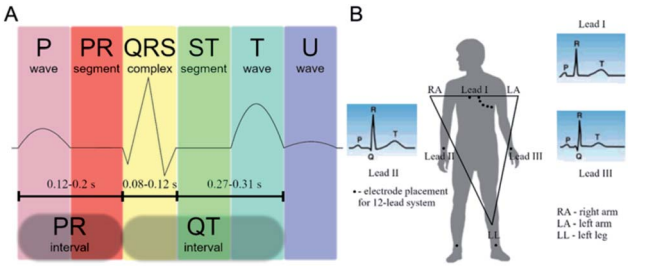

Fig. 2 (A) ECG of a heart in its normal (healthy) sinus rhythm – a simplified overview with the distinct features; (B) placement of the ECG electrodes by the Einthoven's triangle.

over the threshold – causes migration of sodium cations throughout the sodium channels. The result is a lowered negative charge inside the cell. When the atria and the ventricles are stimulated, the P-wave and the QRS-complex can be recorded, respectively. After depolarization Na^+ channels close and the K^+ channels open. Potassium ions leave the cellular membrane and the potential returns to its resting values. This process – called repolarization – is seen as the T-wave on the electrocardiogram.[32]

The electrode placement is selected on the basis of Einthoven's triangle (Fig. 2B). Typical ECG equipment requires ten electrodes (12-lead ECG) connected to chest, arms and legs.[33] It should be emphasized that attaching such electrodes is time-consuming and can be performed only by a trained healthcare professional and, obviously, it cannot be used by patients at home for long-term monitoring. Importantly, as patients could display only transient symptoms, ECG would not capture them during the standard ECG protocol and such problems would require the continuous ECG monitoring. Holter monitor is a response to those needs as a device for 24–48 h cardiac monitoring. The number of electrodes is here less than in the conventional ECG system although the simplification of device reduces sensibility of the signal measurement. Another problem is related to the electrodes. The most commonly used electrodes are the gel-type Ag/AgCl. In principle, gel improves quality of the recorded signals; however, it often causes skin irritation. Also, wet electrodes adhere to the skin causing thermal discomfort of the patient. Furthermore, drying of the electrodes means degradation of the ECG signal.[34] The electrodes are connected with the recorder by metal wiring – typically six to ten wires worn around the patient's body. Likewise, wires can cause skin irritation and are uncomfortable, especially during long-term recordings. In turn, glued electrodes and wires are sensitive to water, which renders taking a shower during the monitoring (putting on and taking off the electrodes is troublesome since the electrodes must be placed in the appropriate positions).

The ECG electrodes mainly include metals (silver, copper), conductive polymers (polyaniline, poly(3,4-ethylenedioxythiophene), poly(3,4-ethylenedioxy-pyrrole, *etc.*) and carbon allotropes (carbon black, graphene, and CNTs). Metals though display high electrical conductivity in bulk, they are in the same time non-stretchable/inextensible, lack in natural

adhesivity and could cause skin irritation upon prolonged contact. On the other hand, conductive polymers upon careful surface preparation or pre-treatments are prone to effectively interact with the human skin (in terms of contact area and electrical contact) and exhibit enhanced biocompatibility with maintained high electrical conductivity. In the same time, conductive polymers are characterized by poor inherent mechanical flexibility which is a factor which cannot be overestimated in the design of ECG signals registered upon movement. Furthermore, most of conductive polymers require doping, and – what is critical for effective and economic processing – decompose at temperatures lower than their melting point, and have poor solubility in typical solvents due rigid backbone structure and lower molecular weights. And eventually, carbon materials arrive as the best suited for applications as ECG electrode – mainly due to their outstanding mechanical and electrical performances, low-cost, high chemical/thermal stability and biocompatibility.

Having in mind the above, ECG cannot be envisaged as a simple technique measuring electrical potential differences naturally occurring in the body; the overall image is more complicated and the competitive solutions must meet the demanding criteria of reliability in the rapid detection and diagnosis of cardiological problems (Fig. 3). The ECG electrodes, apart from the accurately detecting changes in the skin surface voltage, should exhibit an excellent to-skin adhesion. Moreover, as the electrodes also convert ionic into electron current,[35] not only the electrode material and geometry affect the signal acquisition, but also their position.[36,37]

Fig. 3 The requirements for novel ECG materials.

3. CNTs as the key component of ECG systems – structure–properties relationship

Why CNTs with all their tremendous potential are still not extensively present in everyday electrical applications including textronics and smart textiles for ECG? The answer should start with an explicit distinction that all of the CNT properties are driven by their molecular architecture and 3D-assembly. Hence, the crucial step that has to be done is to bring those excellent properties recorded for the individual CNTs into the macroscale.

3.1 Structure of CNTs

The key criterion describing CNT morphology is the number of walls. Single-walled CNT (SWCNT) can be considered as a seamless hollow cylinder being a rolled-up graphene sheet. On the basis of crystallographic structure, one can distinguish three types of ideal SWCNTs depending on how the graphene sheet was 'rolled-up': zigzag, armchair and chiral.[38] In the zigzag conformation, two opposite C–C bonds of each hexagon are parallel to the tube axis, whereas in the armchair conformation the C–C bonds are perpendicular to the axis. In all other arrangements, the opposite C–C bonds lie at an angle to the tube axis, resulting in a so-called chiral nanotube.[39] One can imagine that multi-walled CNT (MWCNT) is a set of SWCNTs which are coaxially stacked. Distance between SWCNTs 'contributing' to MWCNT is close to the interlayer distance in graphite (~0.34 nm).[40] It is worth to note that since 2006 MWCNTs having 2–5 walls have been considered as a special case of CNTs called few-walled CNTs (FWCNTs) due to the explicit inter-tube interactions. Contrary to larger MWCNTs, FWCNTs can retain remarkable electronic and optical properties of the inner walls.[41]

As it is mainly electroconductivity which makes CNTs the 'electrode + wiring' material for ECG acquiring, one must analyse CNT electronic properties as a function of structure and morphology. MWCNTs are usually considered as zero bandgap semiconductors while SWCNTs may be metallic or semiconducting (with a bandgap in the range of 0.4 to ~2 eV). The difference originates in the fact that, in case of MWCNTs, conduction at low voltages proceeds through the outer shell as responsible for the zero band-gap (similarly to graphite). In the case of SWCNTs, electrical properties depend strongly on their diameters and chiral structure, *e.g.* for typical diameters only armchair nanotubes can be metallic.[42] The more detailed discussion of electrical properties of CNTs and their relation with electronic structure can be found in the next section.

What makes CNTs attractive almost 30 years after their discovery and in the age of the growing interest in graphene? CNTs are now the main counter-candidate of graphene for biomedical (and not only) applications. Let us take a look at Table 1 and combine those outstanding CNT physical properties with availability which is incomparably greater than that for any other nanocarbon family representative. Analysis of Table 1

Table 1 Physical properties of individual CNTs

Property	SWCNT	MWCNT	Ref.
Tensile strength	~1 TPa	~1–1.2 TPa	43 and 44
Thermal conductivity (along the axis)	~1750–5800 W m^{-1} K^{-1}	>3000 W m^{-1} K^{-1}	45 and 46
Bandgap	0 eV (metallic) 0.4–2 eV (semiconducting)	0 eV	47 and 48
Electrical resistivity (along the axis)	10^{-6} Ωm		49 and 50
Max. current density (along the axis)	10^{7} to 10^{9} A cm^{-2}		51 and 52

clearly shows that individual CNTs can virtually compete with the materials being 'leaders' of almost each 'category'. For example, copper, which is often considered as an excellent material in heat transfer related applications exhibits the thermal conductivity of just 385 W m^{-1} K^{-1}.[53] On the other hand, carbon fibre, which was for the long time described as *the strongest man-made fibre*, has a tensile strength of just 6370 MPa. Moreover, maximum current density for copper is almost 10^{6} A cm^{-2}.[54] In the case of electrical conductivity along the nanotube axis, CNTs can successfully rival steel (6.9×10^{-7} Ωm).

3.2 Origins of CNT electrical conductivity

There has been a strong interest in electronic properties of CNTs since the very first theoretical predictions in 1992.[55,56] One of the most tempting hypotheses was that CNTs at the metallic bands may act as ballistic 1D conductors. This phenomenon implies that there is no electron scattering over the CNT length.[57] In other words, the electrons remain in local equilibrium as they enter and exit contact pads. Electrical properties of CNTs are strictly related to their electronic structure based on conjugated π-electronic system, thus it is convenient to start the considerations with simpler and more theoretically tractable SWCNTs.

3.2.1 Electrical conductivity of SWCNTs. In order to understand the electrical properties of CNTs, one should begin with their 'precursor' *i.e.* graphene nanoribbon (GNR) (Fig. 4). The quantum electronic states of graphene are purely 2D with a single allowed value for $\mathbf{k}_z$ and almost continuously varying moments in the plane ($\mathbf{k}_x$, $\mathbf{k}_y$) ($\mathbf{k} = (\mathbf{k}_x, \mathbf{k}_y)$ is the momentum. Following the standard Fermi liquid model, a 2D free-electron system has virtually the same parabolic energy dispersions as the 3D system. The only difference is that surfaces of constant energy (isoenergetic) are geometrically represented in cross-section as circles or curved lines instead of the typical spheres and spheroids. As it can be seen in Fig. 4A, many of the constant energy surfaces of graphene are circular lines, but there is a distinct geometry at corners $\mathbf{k} = \mathbf{K}$ (points indicated by vector $\mathbf{K} = (2\pi/a)(1/3, 1/\sqrt{3})$ (where a is the lattice constant given by $a =$ 0.246 nm) of the first Brillouin zone which is a uniquely defined primitive cell in the reciprocal lattice.[58] The two bands derived from π and π* states of two carbon atoms cross themselves with almost perfect linear dispersion at each corner, thus constant-energy surface becomes a discrete point which lie exactly at the graphene's Fermi energy E_F.

Both carbon atoms in the unit cell contribute with one p_z electron to the crystal, therefore it seems clear that for the band composed of p_z orbitals each is filled to the band edge **K**. This in turn results in E_F lying exactly at the band intersection. While typical metals might have Fermi surfaces with many quantum states available, graphene has a Fermi surface which is in fact a set of Fermi points. It results in a behaviour which may be considered as zero-bandgap semiconductor.[61] Further quantization of graphene lead to 1D GNRs which are sliced narrow strips from the 2D graphene sheet. In GNRs, the allowed electronic states constitute a 'band' sliced from the graphene band structure. When GNR width is equal to finite number (N) of carbon atoms, then N parallel sub-bands contribute to the complete set of allowed states. As it can be seen in Fig. 4B, slicing of graphene sheet may result in the materials of remarkably different electronic properties.[60] 'Cutting' the graphene sheet in different directions results in semi-conducting behaviour of GNR. It can be assumed that in order to describe GNRs in terms of their electronic properties both parameters should be considered: width and the angle of the strip with respect to the hexagonal atomic lattice.[62]

Generally, SWCNTs are isoelectronic with GNRs with some subtle differences. In fact, due to the presence of the edges of GNRs which dictate boundary conditions of a hard-wall potential, the sub-bands of SWCNTs fit even more accurate the above discussed model than flat GNRs. The metallic GNR structure

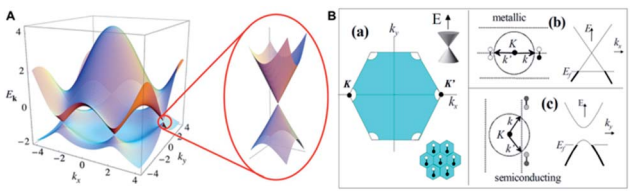

Fig. 4 (A) Schematic depiction of electronic band structure of a graphene sheet. The Fermi level E_F intersects the corners of Brillouin zone; this figure has been reproduced from ref. 59 with permission from American Physical Society, Copyright 2020; (B) 1D quantization of graphene band structure resulting in GNRs: (a) filled states in the first Brillouin zone of a single graphene sheet (the sheet consists of two carbon atoms per unit cell – lower right inset). The Fermi circle around K point, the allowed k vectors and their dispersions are shown in (b), and (c) for a metallic and semiconducting GNR (SWCNT), respectively. The dumbbells represent molecular orbitals comprising the states, with white–white, white-black and grey dumbbells representing bonding, antibonding and mixed orbitals respectively. This figure has been adapted from ref. 60 with permission from American Physical Society, Copyright 2020.

discussed above may be considered as an equivalent of metallic (armchair) SWCNT. It should be kept in mind that for SWCNTs of diameter lower than 1 nm electronic states will be altered due to the curvature-induced strain. While considering electronic properties of SWCNTs it is very convenient to describe them using the so-called chiral vector which is composed of two primitive lattice vectors $\mathbf{c} = \mathbf{na_1} + \mathbf{ma_2}$ (Fig. 5A) and which, in simple words, describes how the GNR (rolled-up to produce SWCNT) was sliced from the initial 2D graphene.[63–65]

In a simplified model (negligible strain effects related to curvature), all SWCNTs with $\mathbf{n} = \mathbf{m}$ are metallic and their sub-bands are depicted in Fig. 5B. For SWCNTs with $n \neq m$ the sub-band intersecting k will not cross **K** point, however one of the remaining parallel sub-bands may intersect **K**. It may be simply evidenced that when difference between n and m can be divided by 3, one of the diverse allowed sub-bands intersects the **K** point and causes metallic behaviour of SWCNT. Therefore, it can be stated that 1/3 of all SWCNTs are metallic and the remaining 2/3 are semiconductors (Fig. 5C).

The SWCNTs of diameter D [nm] being semiconductors have defined bandgaps E_g which are independent of specific values of n and m and can be calculated using the simple equation $E_g \cong 0.85/D$ eV. Interestingly, metallic SWCNTs were proved experimentally to act as ballistic conductors when both contact resistance and elastic scattering were limited.[66]

3.2.2 Electrical conductivity of MWCNTs. MWCNTs are much more complex systems than graphene, GNRs or SWCNTs. The distance between SWCNTs contributing to MWCNT is too large for electronic 'communication' (*i.e.* band overlapping) of the walls just as in the case of graphite, so the individual layers can be virtually considered as a set of independent SWCNTs with the properties described above. It seems quite simple but the situation is still much more complicated. Each wall may be of different chirality, thus MWCNT may be imagined as a coaxial wire with many alternating layers. It is assumed that the diameter-dependence of bandgap mentioned above is preserved, therefore MWCNT can exhibit radial bandgap variation from wall to wall.[67] While non-metallic FWCNTs with diameter of 2 nm in the absence of walls of metallic chiralities exhibit bandgap of ~0.3 eV, the MWCNT of outer diameter of 20 nm would have bandgap of 0.03 eV, so at room temperature, due to small bandgap ($k_BT > E_g$) its outer wall would practically conduct regardless of chirality. It is believed that, in general, at low temperatures and low bias – the conduction in MWCNTs is exclusively determined by the outer wall. Under those conditions, MWCNTs behaviour is much like that of large diameter SWCNTs (including quasi-ballistic conduction).[68] However, measurements at room temperature clearly indicate that contribution of inner shells can be limiting factor for some electronic applications. For example, it was demonstrated that low diameter MWCNT of a semiconducting outer shell could be gated in electrostatic fields and – because of metallic inner wall leakage – could not be turned-off.[69]

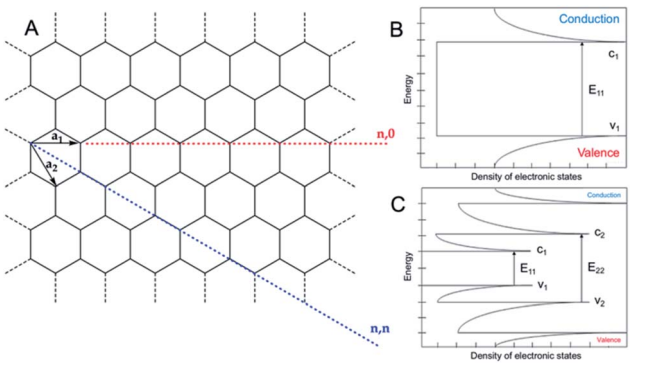

Fig. 5 (A) Depiction of CNT chiral vector $\mathbf{c} = \mathbf{na_1} + \mathbf{ma_2}$; (B) density of states of metallic and (C) semiconducting SWCNTs; v – valence band, c – conduction band.

3.2.3 Mechanical, optical and thermal properties of CNTs. Individual CNTs are the strongest materials ever discovered.[70] Those outstanding mechanical properties are connected with the strength of the multiple sp^2-bonds.[71] As compared to steel, individual CNTs have six times lower density (*ca.* 1.3 g cm^{-3}),[72] five times higher stiffness under tensile (Young's modulus *ca.* 1 TPa)[73,74] and fifty times higher tensile strength (*ca.* 63 GPa).[74,75] The shear modulus for SWCNT and MWCNT is 870.7 GPa[76] and 500 GPa,[77] respectively. Those values are higher than for diamond (478 GPa) and much higher than for steel (79.3 GPa). Poisson's ratio (the ratio of transverse contraction strain to longitudinal extension strain in the direction of stretching force) for SWCNT is 0.2–0.4 (and decreases with the SWCNT diameter). For MWCNTs, Poisson's ratio is 0.25–0.35 and is practically independent of the number of walls. Buckling load for individual SWCNT is about 5–100 nN and is inversely proportional to aspect ratio. For MWCNT, the buckling load is between 5 and 150 nN and is proportional to the MWCNT diameter.[78] The sp^2-bonds can rehybridize from sp^3-bonds as they are strained which makes CNTs resist to breaking upon strain.[79]

Optical properties of SWCNTs are connected to electronic transitions within one-dimensional density of states with non-continuous function of energy.[80] Because of one-dimensional character in the density of states, the 'spikes' emerge called van Hove singularities.[81] Only optical transitions between v_1–c_1 and v_2–c_2 are permitted (v – valence band, c – conduction band).[82] Energy difference between the states depends on the CNT structure.[83] Optical absorption by CNTs originates from those electronic transitions.[84] Additionally, some of CNTs act as black body exhibiting absorbance around 1 from 200 nm to 200 μm.[85]

Similarly to diamond and graphite – the other members of the carbon allotrope family – CNTs also exhibit superior thermal properties. They are characterised by high thermal conductivity, *e.g.* for (10,10)-SWCNTs thermal conductivity is *ca.* 6600 W m^{-1} K^{-1} at room temperature,[86] as a result of large phonon mean free path.[87] At room temperature thermal conductance for SWCNTs is linearly proportional to the diameter, while for MWCNTs to the square of diameter.[88] As observed for MWCNTs, thermal conductivity increases when the number of walls decreases.[89] CNTs have much higher conductivity along the tube, compared to the perpendicular direction.[90] Thermal conductivity increases also with the increase of CNT length and

is higher for defect-free CNTs. For SWCNTs at low temperatures (near 0 K), thermal conductivity increases linearly with the increase of temperature (ballistic transport). With the further increase in temperature, thermal conductivity is governed also by additional phonon modes. Thermal conductivity reaches the maximum value close to room temperature. Upon rising temperature, further reduction of thermal conductivity proceeds due to domination of the photon scattering.[91] For CNTs films, higher values of thermal conductivity are obtained for more densely packed samples and of the better alignment.[92] It can be therefore summarized that, as all of the critical CNT properties strongly depend on 3D-assembling, the range of characteristics may cover practically the whole scales of given values in the several orders of magnitude.

4. Manufacture of self-standing CNTs and CNT composites

In this section, CNT-based macroscopic systems are discussed as key components toward electrical applications. Two types of such systems can be generally considered: (1) CNT-based films and wires which integrity is provided by weak intermolecular interactions (van der Waals forces, π–π stacking, *etc.*) between CNTs; that kind of integrity is achievable during processing, and (2) composite materials in which CNTs are dispersed within a polymeric matrix ensuring structural integrity of the material. It is worth to note that a special case of composites are paints and inks for various printing methods (screen printing, inkjet printing, gravure printing, *etc.*) as they form composite layer on a support after *e.g.* solvent evaporation.

4.1 Manufacture of CNT-only materials

In general, two groups of methods of free-standing CNT macro-assembly preparation can be recognized. First – using the so-called wet-chemistry and second, based on solid phase transfer. Structural integrity of materials obtained by those methods is provided by weak van der Waals forces between individual tubes. Quite oddly, these are the same interactions which are responsible for hampered dispersibility and the overall usability of CNTs in electrically conductive composites.

4.2 Wet-chemistry methods

This multi-step approach starts with dispersion of CNTs in the appropriate solvent. De-bundling of the material may be facilitated by covalent or non-covalent functionalization. Fine dispersions containing CNTs are further transferred to the (temporary) substrate using dip coating, spray coating, spin coating, membrane filtration (in this case the membrane act as a substrate), and they can eventually be directly spun.[93–97] After evaporation of solvent, the substrate is removed what results in a desired CNT macro-assembly. An interesting example of application of this method was demonstrated by researchers from the Rice University as they obtained highly aligned and densely packed CNT films using simple filtration of aqueous CNT dispersions. They concluded that in order to achieve spontaneous alignment in the film: (a) the concentration of surfactant has to be below the critical micelle concentration; (b) the CNT concentration must be below a threshold value which depended on the parameters (aspect ratio, purity) of CNTs used; (c) the filtration has to be carried out in a controlled (slow) manner.[98]

4.3 Solid-phase transfer

Solid phase transfer single-step methods[99] can be considered as a variant of typical *c*-CVD process. Carbon source together with catalyst and (unnecessarily)[100] sulphur promoter are injected into the furnace (1050–1200 °C). Under certain conditions, in the hot zone of the reactor, an aerogel consisting of CNTs is formed. This aerogel is further continuously drawn out of the furnace and collected using a winder (virtually any rotating object) what results in obtainment of horizontally aligned CNT films or the so-called carbon nanowires (CNWs).

4.4 Manufacture of CNT-based composites/films and hybrid materials

Generally, there are three most important methods of CNT-based composites preparation: solution mixing, melt mixing and *in situ* polymerization. All of them need to deal with the major drawbacks of CNTs as nanofillers – poor dispersibility in essentially any system and tendency to formation of bundles which are caused by weak but widespread inter-tube interactions (van der Waals attraction, π–π stacking). One of the methods to weaken those forces is functionalization of CNT surface[101–103] but this approach typically yields nanotube products of deteriorated characteristics.

The simplest and the most popular method for composite preparation is solution mixing where both nanofiller and polymeric matrix are introduced to a suitable solvent. When the mixture becomes homogenous, the solvent is evaporated and the composite (predominantly – film) is formed. A wide range of composites has been prepared using this method as the final product may be obtained by *e.g.* spin-coating, electro-spinning and numerous printing techniques, such as *e.g.* screen printing.[104–108] In fact, the intermediate product (*pre-composite*) obtained during the solution mixing may be considered as an ink if it meets the requirements of particular printing method, *i.e.* adhesion to the substrate, mean particle size, viscosity and boiling point of the solvent. Despite the abovementioned functionalization, a crucial factor for obtaining fine CNT dispersions is selection of a method used to introduce nanotubes to a solution. The most commonly used ones are ultrasonic agitation and high-shear mixing.

Solution mixing method is limited by solubility of the polymers. To attenuate this obstacle the melt processing may be used for thermally stable polymers (thermoplastics) such as polypropylene (PP), polystyrene (PS), polycarbonates (PC), *etc.*[109–112] In melt processing the polymer is blended with CNTs while being a liquid. It can be melted before blending or mixed in a solid state and then melted. The major disadvantage of this technique is high viscosity of melted polymers which makes it difficult to achieve uniform distribution of CNTs within the matrix.[113]

In another convenient method, *i.e. in situ* polymerization, CNTs are dispersed within monomer matrix not necessarily in the presence of the solvent. Once the CNTs are uniformly distributed in the system, polymerization starts. *In situ* polymerization is beneficial as in some cases it can enable anchoring of polymer chains on CNTs' surface. As obtained polymer–CNT hybrid macromolecules are usually better dispersed within the composite. Moreover, the advantage of *in situ* polymerization is that it can be used for the polymers which are not processible by solution mixing or melt mixing. On the other hand, it should be kept in mind that since CNTs are radical-scavengers the molecular weight of polymer synthesised in the presence of CNTs is usually lower,[114] also prolonged and/or less-developed cross-linking of pre-polymer blends can occur. Examples of *in situ* polymerization include *inter alia* MWCNT–PS, MWCNT–polyurethane (PU) or MWCNT–PE systems.[115,116]

5. CNTs in electrocardiography – overview of solutions and characteristics

Polydimethylsiloxane (PDMS) is the most exploited polymer in the CNT-composites in ECG systems as its properties can be tailored by molecular weight and additives. PDMS is inert to skin and considered widely as non-toxic. PU and acrylic resins were also used. All of the matrices combined with CNTs are found in Table 2 presenting the comprehensive analysis of CNT-based solutions for electrocardiography.

The key property from the ECG electrode point-of-view is high electrical conductivity, hence metal have been most often chosen material for ECG electrode preparation. However, as mentioned earlier, metal electrodes suffer from higher density, low biocompatibility and susceptibility to corrosion, therefore, multi-functional and environmentally stable metal substitutes are needed; CNTs are indeed very promising candidates in this field. As can be seen in Table 2, addition of CNTs to the electrically insulating matrix certainly improves electrical performance of composites. The composites and films/coatings can be used as both ECG electrodes and conductive paths. Nevertheless, it is essential to attune type and concentration of CNTs in the selected polymer matrix, connect the expected properties with the components and manufacture route, and eventually miniaturise/balance coating dimensions. MWCNTs were the most frequently selected as conductive fillers, but SWCNTs also represent prospective candidates, particularly in the transparent electrodes. On the other hand, purely metallic SWCNTs are from one to two orders of magnitude more expensive. In a few cases CNTs were modified before addition to polymer. While oxidation of CNTs could improve dispersibility in polymer matrix and allow forming conductive 3D network, it may also substantially destroy sp^2-carbon shells hence furnish coatings of impaired characteristics. Further, choice of the appropriate concentration is typically a trade-off between electrical (one must cross percolation threshold) but also mechanical properties with flexibility and adhesion as the most important ones. This is in fact much more complex problem requiring addressing physicochemical compatibility of CNTs and matrix – CNT type and concentration needs to be selected individually as a function of matrix and manufacture technique. Here, viscosity of the pre-polymer blend is crucial and derives not only from the matrix itself but predominantly from surface area and entangling of nanotubes. Also, if the energy of mixing is too high, one might obtain cut, defectuous or to-graphene exfoliated nanotubes of the entirely degenerated properties. Finally, the coating area emerges also as important since it cannot compromise the patients' comfort. Overall, the manufacture itself should provide time- and operation-stable dispersions of CNTs in the polymer matrices, which enable formation of durable CNT-based electrodes – particularly for long-term applications.

Biocompatibility – understood here more narrowly as safety of the contact of a given object with the human skin – is obviously the *sine qua non* condition for the medical-value ECG solutions awaiting to be approved by the market. Various methods are available for the assessment of biocompatibility of CNT-based ECG electrodes for which toxicity assays, at different levels from cell *via* tissue to organs, play the key role. The methods for toxicity assessment can be further categorized into *in vitro* and *in vivo*. *In vitro* toxicity assays can be subdivided into proliferation, apoptosis, necrosis, oxidative stress and DNA damage assays. The *in vivo* toxicity assessment is performed on animals. The assessment methods for *in vivo* toxicity include biodistribution studies (distribution route to the tissues or organs), clearance (examination of the excretion and metabolism), haematology, serum chemistry and histopathology. For CNT-based electrodes, skin compatibility assays derived from dermatological standards were typically the first-choice tests. In few other cases other tests were applied, *e.g.* human or mouse skin fibroblast cells or keratinocytes.[117–120]

5.1 Polymer and hydrogel electrodes

In order to collate the up-to-date results in the area of CNTs in electrocardiography, one must scan the existing solutions not only qualitatively but first of all quantitatively evaluate what many authors omitted in the works. And while the topic of this review spans actually from 2012, earlier works could be here also recalled as the inspiration for the future works. And in one of the earliest works from 2008, Baek *et al.*[148] fabricated a dry electrode on a flexible PDMS substrate. The electrode was connected to Velcro® (hook-and-loop fastener) and placed as a bracelet on the forearm (Fig. 6A). The bracelet centre was equipped with gold electrical contact (thickness 3000 Å) and titanium substrate (thickness 300 Å). The preparation procedure was two-stage: (1) fabrication of the electrode and the base structure, and (2) conjugation of the electrode with the base structure. PDMS electrode did not cause any skin irritation or allergic reaction. The impedance of the electrode was quadrupled than for Ag/AgCl electrode for low (below 100 Hz) and almost the same for the higher frequency range. The impedance decreased in time, probably due to environmental moisture and patient's sweat. ECG signals were measured using PDMS and

Table 2 CNT-based materials for electrocardiography[a]

CNTs outer diameter length	Matrix additive, conc.	CNTs, conc.	Form/assembly thickness	Electrical properties	Biocompatibility tests	Long-term application	Advantages/key features	Disadvantages	Ref.
MWCNTs 80–90 nm, 50 μm	PDMS, AgNPs, 11 wt%	11 wt%	Polymer electrode 0.6 mm	Z = 10–80 kΩ	Skin compatibility	11 days	✓ Signal dependent on CNT conc. ✓ Stability in stationary positions ✓ Self-adhesion ✓ Stability in 5 cycles detach/attach ✓ No long-term irritation to skin	✗ Strong motion artifacts ✗ Metallic additive ✗ High (>4 wt%) CNT content ✗ Lower ECG signal than for Ag/AgCl ✗ Decreasing adhesivity over use	121
MWCNTs 10–40 nm, 1–25 μm	PDMS	1.0, 1.5, 2.0 wt%	Polymer electrode 200–600 μm	$\sigma = 10^{-3.1}$ S m^{-1}	n.d.	n.d.	✓ Signal dependent on CNT conc. ✓ Clear QRS-complex	✗ Weak T-wave ✗ No dynamic testing ✗ Deterioration of mechanics	122
MWCNTs 8–15 nm, 50 μm	PDMS	10 wt%	Polymer electrode thickness n.d.	σ = 26.7 S m^{-1} Z_c = 348 kΩ	n.d.	n.d.	✓ Micropillar enhanced contact area ✓ Stability in stationary positions	✗ Noise during walking ✗ High (>4 wt%) CNT content ✗ No long-term testing ✗ No biocompatibility tests	123
MWCNTs 80–90 nm, 50 μm	PDMS AgNPs, 11–12 wt%	11–12 wt%	Polymer electrode sewed into bra/vest thickness = 0.6 mm	Z = 100 kΩ to 50 MΩ Z_c = 50 kΩ	Skin compatibility	14 days	✓ Signal dependent on CNT conc. ✓ Signal dependent on layer thickness ✓ Stability in stationary positions ✓ Stability in time ✓ No irritation to skin ✓ Washability	✗ Metallic additive ✗ Lower ECG signal than for Ag/AgCl ✗ High (>4 wt%) CNT content ✗ Noise during walking ✗ Motion artifacts in dynamic testing	124
MWCNTs 20 nm, 25 μm	PDMS-Ag, PDMS coating	PDMS : CNT 3 : 7	Polymer electrode thickness n.d.	Z_c = 100–600 kΩ	Skin compatibility	7 days	✓ Signal dependent on CNT conc. ✓ Temperature/humidity stable signal ✓ Attaching/detaching stability ✓ No long-term irritation to skin ✓ Stability in time	✗ Lower ECG signal than for Ag/AgCl ✗ Metallic coating ✗ No dynamic testing	125

Table 2 (*Contd.*)

CNTs outer diameter length	Matrix additive, conc.	CNTs, conc.	Form/assembly thickness	Electrical properties	Biocompatibility tests	Long-term application	Advantages/key features	Disadvantages	Ref.
SWCNTs 0.9–3 nm, <10 μm	Alginate/ polyacrylamide hydrogel	SWCNT film deposited on hydrogel	Hydrogel-based electrode thickness = 40 nm	σ = 100–350 Ω sq^{-1}	n.d.	n.d.	✓ High signal amplitude ✓ Excellent to-skin adhesion ✓ Optical transparency	✗ No dynamic testing ✗ Susceptibility to cracking ✗ Noisy baseline ✗ High costs	126
MWCNTs 20–30 nm, 10–30 μm	PDMS Ag coating	8 wt%	Polymer electrode thickness n.d.	σ = 938.8 mS sq^{-1} Z_c = 524–1000 kΩ	n.d.	n.d.	✓ Signal of medical quality ✓ Signal dependent on the electrode diameter ✓ Dynamic stability	✗ Metallic additive ✗ Noisy baseline ✗ High (>4 wt%) CNT content ✗ Strong motion artifacts	127
MWCNTs 50–85 nm, 10–15 μm	PDMS	4.5 wt%	Polymer electrode thickness n.d.	$\sigma = 10^{-7}$ to 10^{-5} S	n.d.	n.d.	✓ Signal of medical quality	✗ No dynamic testing ✗ Unknown reproducibility	128
MWCNTs 10–40 nm, 1–25 μm	PDMS	1, 1.5, 2, 4.5 wt%	Polymer electrode thickness = 3 mm	$Z_c = 10^3$ to 10^7 Ω $\sigma = 10^{-4}$ to 10 S m^{-1} 1–4.5 wt%	Skin compatibility Cytotoxicity test by culturing skin fibroblast CCD-986sk cells	7 days	✓ Signal dependent on CNT conc. ✓ Signal dependent on the electrode diameter ✓ ECG signal of nearly medical quality ✓ Stable signal over sweating ✓ No long-term irritation to skin	✗ Noisy baseline in dynamic testing ✗ Lower time-stability ✗ Weak QRS- and T-waves	129
MWCNTs 10–40 nm, 1–25 μm	PDMS Metal pattern layer (Au/Ti/ polyimide)	1, 1.5, 2, 2.5 wt%	Polymer electrode thickness n.d.	$Z_c = 10^4$–10^8 Ω σ = 1–16.4 S m^{-1}	Skin compatibility Cytotoxicity test by culturing human fibroblast cells (CCD-986sk) and mouse fibroblast L929 cells	n.d.	✓ ECG signal of nearly medical quality ✓ Signal stability over attaching/ detaching ✓ Waterproof system ✓ No long-term irritation to skin ✓ Washability	✗ Metal additives ✗ No dynamic testing ✗ Lower time stability	130 and 131

Table 2 (*Contd.*)

CNTs outer diameter length	Matrix additive, conc.	CNTs, conc.	Form/assembly thickness	Electrical properties	Biocompatibility tests	Long-term application	Advantages/key features	Disadvantages	Ref.
MWCNTs n.d.	PDMS–PEIE	10 wt%	Polymer electrode thickness nd.	$Z_c = 10^3$ to 10^7 Ω	Skin compatibility	n.d.	✓ Mechanic stability over attaching/ detaching ✓ No long-term irritation to skin	✗ Motion artifacts in dynamic testing ✗ Sensibility to sweating ✗ Unknown reproducibility	132
O-MWCNT [OH] = 12 at% [COOH] = 7.45 at% 20–30 nm n.d.	Acrylic ink	Acrylic resin:MWCNT (1 : 1 or 1 : 2; v/v)	Textile electrode thickness n.d.	n.d.	Skin compatibility	n.d.	✓ Wearable electrode ✓ Non-toxicity	✗ Low quality of ECG signal ✗ Noisy baseline ✗ No dynamic testing	133
O-MWCNT [COOH] = 0.5–3.86 wt% 7–80 nm, 0.5–2 μm	Paper infiltrated Graphite oxide (GO) GO : MWCNTs (5.7 : 1; w/w)	15, 25, 35 wt%	Paper electrode thickness n.d.	Z_c = 30–60 kΩ	Skin compatibility	n.d.	✓ ECG signal of medical quality ✓ Signal amplitude higher than for conventional electrode ✓ No long-term irritation to skin	✗ Noisy baseline after prolonged use ✗ Loss of signal stability for higher MWCNT concentrations ✗ No dynamic testing	134
MWCNTs 5 nm > 100 μm	Polyrotaxane-based gel		Polymer electrode thickness = 50–100 μm	ρ = 10–50 kΩ	Colony-forming assay on hamster fibroblasts (V79) Implant assay on hypodermal tissues of living rabbits	n.d.	✓ ECG signal of medical quality ✓ Amplitude of signal two times higher than for commercial electrode	✗ Moderately irritant ✗ No dynamic testing	135
SWCNTs 1.2–2 nm, 5 μm	PDMS	n.d.	Polymer electrode thickness = 85 μm	$\rho = 10\ \Omega\ sq^{-1}$	n.d.	n.d.	✓ ECG signal of medical quality	✗ Noisy baseline during dynamic tests ✗ Loss of amplitude stability during dynamic tests	136
MWCNTs 8–15 nm, 50 μm	PDMS	4, 5.5, 7, 8 wt%	Polymer electrode thickness = 500 μm	$Z_c = 10^4$ to 10^7 Ω	Skin compatibility Cytotoxicity test on HaCaT cells	7 days	✓ ECG signal of medical quality (for MWCNT conc. >4 wt%) ✓ Prolonged signal stability ✓ No long-term irritation to skin	✗ High (>4 wt%) CNT content ✗ Weak T-wave ✗ Noisy baseline in dynamic testing	137

Table 2 (*Contd.*)

CNTs outer diameter length	Matrix additive, conc.	CNTs, conc.	Form/assembly thickness	Electrical properties	Biocompatibility tests	Long-term application	Advantages/key features	Disadvantages	Ref.
MWCNTs 10–20 nm, 10–20 μm	PDMS	1–20 wt%	Polymer electrode thickness n.d.	ρ = 2–7000 Ω sq^{-1}	Skin compatibility Cytotoxicity test on human primary keratinocyte HaCaT cells	n.d.	✓ ECG signal of medical quality ✓ Equal to neat PDMS biocompatibility of MWCNT/PDMS (6 wt%) ✓ No long-term irritation to skin	✗ Skin toxicity for >6 wt% MWCNT/PDMS ✗ No dynamic tests ✗ No long-term tests	138
O-MWCNTs 70 nm, 120 μm	PVDF	5 mg mL^{-1}	PVDF 'filter' electrode thickness = <0.1 mm	ρ = 37.6 Ω	n.d.	n.d.	✓ ECG signal of medical quality	✗ Noisier baseline ✗ No dynamic tests ✗ No long-term tests	139
MWCNTs 10–30 nm 1–1.5 mm 'forest'	On stainless steel foil substrates	100%	CNT 'forest' 1–1.5 mm 'forest'	ρ = 9 Ω	Skin compatibility	7 days	✓ ECG signal of medical quality	✗ Noisier baseline ✗ Skin irritation ✗ Leakage/transfer of CNTs onto skin after peel-off	140 and 141
SWCNTs 0.9–1.3 nm, 1 μm	Poly(3-hexylthiophene)	0.8 mg mL^{-1}	Conductive fiber thickness n.d.	ρ = 0.65 kΩ cm^{-1} on PET Z_c = 18.6–39.3 kΩ	n.d.	n.d.	✓ Clear QRS-complex	✗ Noisy baseline ✗ High costs of SWCNTs ✗ No long-term tests ✗ No biocompatibility tests ✗ No dynamic tests	142
O-MWCNTs 20 nm, 1.5–3.9 μm	Multi-layer composition: Silicon wafers, silicon oxide, titanium, nickel, gold, MWCNTs	n.d.	3D structural electrode thickness n.d.	Z_c = 1.2 Ω mm^{-2}	Cytotoxicity test on primary hippocampal neural cells	n.d.	✓ Size 1000 times smaller than conventional electrode ✓ Capable of measuring different anatomical regions of the isolated heart ✓ Long-term biocompatibility	✗ Lower amplitude and less detailed signal than for Ag/AgCl electrode	143 and 144
SWCNTs 1.1–1.7 nm, 5–30 μm	Polyurethane	n.d.	Textile electrode thickness n.d.	ρ = 9.4–12 300 Ω cm^{-1}	n.d.	n.d.	✓ P-, T-, U-waves and QRS-complex identical with that of Ag/AgCl electrode regardless of motion states, age, sex and BMI index	✗ Noisier baseline	145
	Ag nanowires (d = 30–35 nm, l = 20–25 um)			Z_c = 10–1000 kΩ			✓ Manufacture of electrode strongly affecting impedance/resistance	✗ Lower signal amplitude than for conventional electrode ✗ No biocompatibility tests	

Table 2 (*Contd.*)

CNTs outer diameter length	Matrix additive, conc.	CNTs, conc.	Form/assembly thickness	Electrical properties	Biocompatibility tests	Long-term application	Advantages/key features	Disadvantages	Ref.
SWCNTs 1–2 nm, 5–30 μm	—	8–20 wt%	Cotton yarn thickness n.d.	σ = 1–90 μS ρ = 50–700 kΩ	n.d.	n.d.	✓ ECG signal of medical quality	✗ No dynamic tests ✗ No washing resistance tests (aqueous ink)	146
MWCNTs 10–30 nm, 10–30 μm	Polyurethane	17 wt%	Conductive path on textile Thickness n.d.	ρ = 350 Ω sq^{-1}	n.d.	n.d.	✓ Higher peak amplitude than the gel electrodes ✓ Recordings similar with the gel electrode	✗ Noisy baseline ✗ Two times higher contacting area ✗ No biocompatibility tests ✗ No dynamic tests	147

[a] *O*-CNTs – oxidized CNTs, n.d. – no data, Z – impedance, Z_c – contact impedance, ρ – sheet or specific resistivity, σ – sheet or specific conductivity.

Ag/AgCl electrodes. No significant differences between the two signals were observed in the patient's rest state (Fig. 6B). However, during walk, the signal deteriorated: the electrode was sensitive to motion because of its high impedance and poor connection between the electrode and ECG extension cable. After prolonged wearing, even more noises were observed. Nevertheless, in this work, the researchers demonstrated the main benefits of using PDMS electrode, *i.e.* flexibility and biocompatibility. PDMS emerged at that time as prospective matrix and support for medical devices. And even if authors used metallic conductors, the typical shortcomings of the classical electrode were overcome, but still there has been revealed a larger space for improvements.

Afterwards, due to reveal of superior characteristics of CNTs, typical metals were started to be considered as fully replaceable by the former ones. And so, Lee *et al.*[122] elaborated a novel CNT-based electrode. They examined the effect of MWCNT (d = 10–40 nm, l = 1–25 μm) concentration (1.0, 1.5, 2.0, 4.5 wt%) in PDMS obtaining uniform thin films by spin-coating. The lowest CNT concentration corresponded to very low (<0.01 S m^{-1}) while a higher to the increased electrical conductivity of the composites, but also to reduced flexibility. Composites (1.0, 1.5 and 2.0 wt%) were used for the preparation of ECG electrode (Fig. 6C) but flexibility of the composite with 4.5 wt% of CNTs emerged as deficient and impractical. ECG electrodes were placed on the forearms and the left leg of patient and compared with the (standard) Ag/AgCl electrode. For the electrode containing only 1 wt% of CNTs no signal was observed. For the composite with 1.5 wt% of CNTs, ECG signal was successfully acquired and had similar parameters (amplitude, QRS complex) as for the standard electrode. Importantly, for the higher CNT concentration the signal amplitude was improved. These studies showed that there was a clear and positive relationship between CNT concentration in the composite and its electrical properties. However, CNT concentration affected not only electrical properties but also flexibility of composite. It became clear that a balance has to be struck between high electrical conductivity and the mechanical performance.

Liu *et al.*[121] also used PDMS as the polymer matrix. The electroconductive components were MWCNTs (d = 80–90 nm, l = 50 μm, 11 wt%) and Ag nanoparticles (NPs) (d = 80–90 nm, 11 wt%). Both nanomaterials were dispersed in ethanol by ultrasonication. Next, PDMS monomer was added to the dispersion and all components were magnetically stirred for 2 h. The solvent was removed by mechanical stirring on a hot plate and then heating in an oven. Finally, the mixture was stirred with a glass rod with curing agent Sylgard® 184A (PDMS monomer : curing agent 10 : 1). Ag NPs improved conductivity and flexibility of the electrode. The thickness of self-adhesive electrode was 0.6 mm while its impedance was ten times higher than for Ag/AgCl and was changing in time irregularly. ECG signal was stable in time (Fig. 6D), but again strongly dependent on the patient's motion – even slight changes of body position from sitting to standing led to changes in the baseline and artefacts.[149] This solution was proposed as an improvement of the former research in which concentration of CNTs was two times lower. Yet again, at higher CNT

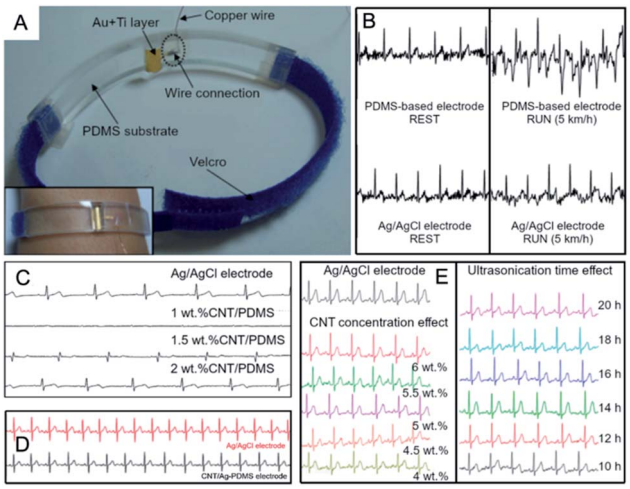

Fig. 6 (A) ECG bracelet and ECG signals for PDMS-based electrode; adapted from ref. 148 with permission from Elsevier, Copyright 2020; (B) ECG signals for electrodes with CNTs compared to Ag/AgCl electrode during rest and run tests; adapted from ref. 148 with permission from Elsevier, Copyright 2020; (C) ECG signals for electrodes with different CNTs concentration compared to Ag/AgCl electrode; adapted from ref. 122 with permission from Springer, Copyright 2020; (D) ECG signals for CNT/Ag-PDMS electrode compared to Ag/AgCl; adapted from ref. 121 with permission from Taylor & Francis, Copyright 2020; (E) effect of CNT concentration and ultrasonication time on ECG signal; adapted from ref. 122 with permission from Springer, Copyright 2020.

concentrations led to the loss of electrode flexibility.[150] Similarly to Liu,[121] Lee studied the effect of CNT concentration and the same results were received (Fig. 6E). Here – additionally – the influence of ultrasonication time on ECG signals was evaluated.

The ECG signal amplitude increased slightly with ultrasonication time (from 10 to 16 h) while its amplitude further decreased after 20 h due to destruction of the CNT structure, nanotube re-agglomeration and weakening the nanotube-matrix bonding. This behaviour in total reduced conductivity of the electrode and signal quality. These findings indicated that not only concentration but also method with optimized conditioning had an impact on the ECG characteristics.

In 2017, Liu *et al.*[124] implemented those electrodes into a bra (Fig. 7A) which emerged as non-irritating for skin after a two-week and functional in rest/exercise test (Fig. 7B). Each electrode was a 0.4 or 0.6 mm-thick 4 cm^2-square. In each case the signal (which amplitude increased with the thickness and CNT loading) was of the medical quality but on walking signal-to-noise ratio significantly decreased which was also found in the case of standard electrode. It is worth to mention that the work involved a female patient. Hence, the natural redirection of the mode of implementation could be amalgamation of the electrode with textiles/clothes which could solve the problem of the loss in electrode-skin contact upon motion.

Peng *et al.* proposed a step forward in this area[123] fabricating a PDMS–MWCNTs (d = 8–15 nm, 50 μm) electrode densely terminated with surface micropillars. PDMS ensured the excellent flexibility, while micropillars the increased electrode-

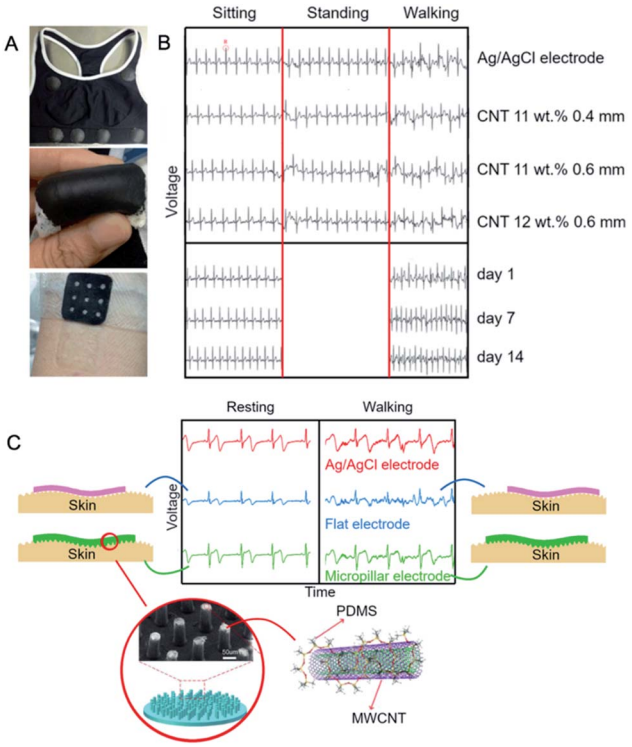

Fig. 7 (A) A photograph of the wearable electrode indicating its flexibility (top), woman's vest with the wearable electrode (middle) and skin compatibility test: no skin irritation was observed at either electrode contact area (bottom); (B) the effect of CNT concentration, layer thickness and wearing time on the ECG signal; figures adapted from ref. 124 with permission from Elsevier, Copyright 2020; (C) ECG for flat *versus* micropillar PDMS/MWCNT electrode and the reference Ag/AgCl electrode; adapted from ref. 123 with permission from Elsevier, Copyright 2020.

skin contact area. Electrical conductivity of the composite equalled 50 mS m^{-1} and 26.7 S m^{-1} for 0.4 wt% and 10 wt% MWCNTs, respectively. For comparison, ECG signals were recorded for standard Ag/AgCl as well as for both flat and micropillar MWCNT/PDMS electrodes. The authors found no differences in the ECG signals for all of the three types of electrodes at resting (Fig. 7C) but, critically, the signal amplitude recorded for the flat electrode was lower due to the weaker skin-electrode contact. Further, during motion in this case the ECG signals deteriorated while for standard and micropillar

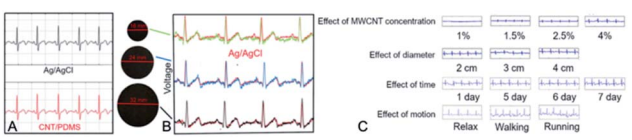

Fig. 8 (A) ECG signals for CNT/PDMS and Ag/AgCl electrodes; adapted from ref. 138 with permission from Elsevier, Copyright 2020; (B) the effect of MWCNT/PDMS electrode diameter on the ECG signals compared to ECG signal obtained from the wet Ag/AgCl electrode; adapted from ref. 127 with permission from Elsevier, Copyright 2020; (C) the effect of MWCNT concentration, electrode diameter, wearing time and motion on ECG signal for MWCNT/PDMS electrode; adapted from ref. 129 with permission from IEEE, Copyright 2020.

electrode, the P-, QRS- and T-waves were distinguishable and the signal-to-noise ratios adopted values higher than for the flat electrode. Many micropillars due to electrode-skin contact improvement allowed for long-term signal recording during movement better than previous flat electrodes.

Jung *et al.*[125] prepared a dry self-adhesive electrode from a MWCNT–PDMS (7 : 3) composite (MWCNT: d = 5–10 nm, l = 25 μm). The electrode was biocompatible and although revealed tripled impedance than for the standard electrode, it displayed a considerably enhanced conformal contact. The ECG signal was coherent with the ECG signal for Ag/AgCl electrode (richer in noises) and neither changes during attaching/detaching tests no signal degradation was observed in 7 days.

Kim *et al.*[138] manufactured MWCNT–PDMS nanocomposites containing 8 wt% of MWCNTs (d = 10–20 nm, l = 10–20 μm). The proposed method of manufacturing involved five steps, was fast (~6–8 h), and cost-effective (1–5 USD per g). The material was biocompatible, flexible, and elastic. The ECG signal recorded from three electrodes (left and right arm) prepared therefrom was essentially identical to the one recorded for the standard Ag/AgCl electrode (Fig. 8A).

Chlaihawi *et al.*[127,151] also fabricated printed, flexible and wearable dry MWCNT–PDMS electrodes (MWCNTs: d = 20–30 nm, l = 10–30 μm) of different nanotube concentration (2, 4, 6 or 8 wt%). Sheet electrical conductivity for those composites ranged correspondingly from 8.3 mS sq^{-1} (2 wt%) to 938.8 mS sq^{-1} (8 wt%), therefore, the latter one was selected for the electrode preparation. ECG electrodes were prepared *via* a two-step procedure. In the first step, Ag ink was screen-printed on a flexible poly(ethylene terephthalate) (PET) substrate and MWCNT/PDMS composite was bar-coated there onto. Three electrodes of different diameters (thickness 285 μm) were tested (16 mm, 24 mm and 32 mm) all enabling recording clear QRS complexes (Fig. 8B), however, the largest electrode had the highest amplitude and signal correlation (0.95) with the standard Ag/AgCl electrode. Moreover, 32 mm-electrode displayed a better performance while tested in motion as compared to the standard electrode. Similarly, Kalra *et al.*[128] used PDMS containing 4.5 wt% of MWCNTs (d = 50–85 nm, l = 10–15 μm). And while conductivity of the composite was still ten times lower than for Ag/AgCl electrode, the acquired ECG signals were practically indistinguishable from those obtained using standard electrode.

Using the same filler-matrix system (MWCNTs: d = 10–40 nm, l = 1–25 μm), Jung *et al.*[129] scanned operation of ECG electrodes as a function of MWCNT concentration (1, 1.5, 2, 4 wt%) as well as electrode diameter (2, 3, 4 cm) and thickness (1, 2, 3 mm) (Fig. 8C). The highest electrical conductivity was found for the highest loading (10 S m^{-1}) while the electrode-skin contact impedance was highest for the smallest electrode. For all electrodes this impedance was strongly depended on frequency. The amplitude of ECG signals was increasing with MWCNT concentration. Overall, the larger electrodes corresponded to the enhanced quality of the signal whereas thickness effect was not as significant as for diameter- and concentration-based relationships. Importantly, ECG signals upon motion emerged as stable in time, nearly noiseless and identical as for the standard electrode.

Lee *et al.*[130,131] developed an interesting epidermis-like MWCNT–PDMS electrode capable of repeated self-adhesion onto skin. Apart from MWCNTs (d = 10–40 nm, l = 1–25 μm 1.0–2.5 wt%), the electrode contained also gold, titanium and platinum. It was a four-layer, few hundred micron-thick structure including adhesive PDMS (aPDMS), MWCNT/aPDMS, Au/Ti/polyimide and PDMS. The roles of the layers were as follows: aPDMS improved adhesivity, MWCNT/aPDMS transmitted signals to the metal layer, metal layer served as an

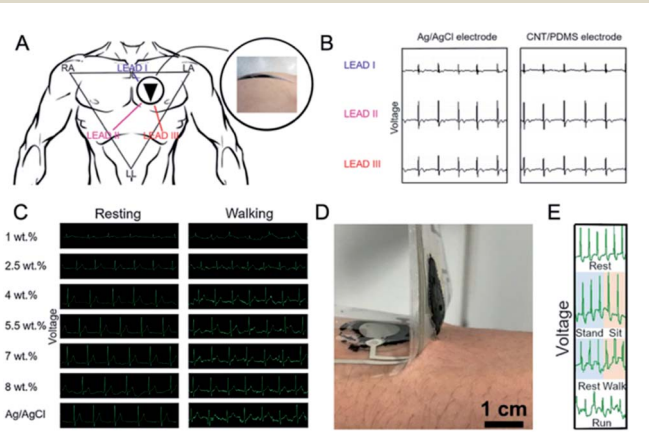

Fig. 9 (A) Placement of the ECG electrodes to the left chest. Triangle shaped RA, LA and LL electrodes represent leads I, II and III and ECG waveforms; (B) recorded with leads I, II, and III for the Ag/AgCl, and dry MWCNT/aPDMS electrodes; these figures have been adapted from ref. 130 and 131 with permission from Nature Publishing Group, Copyright 2020; (C) ECG signals upon resting and walking for various MWCNT concentrations in PDMS; adapted from ref. 137 with permission from Taylor & Francis, Copyright 2020; (D) photograph of adhesion between the MWCNT/PDMS electrode and skin; (E) real-time ECG signal for CNT/aPDMS electrode during motion; these figures have been reproduced/adapted from ref. 132 with permission from The Japan Society of Applied Physics, Copyright 2020.

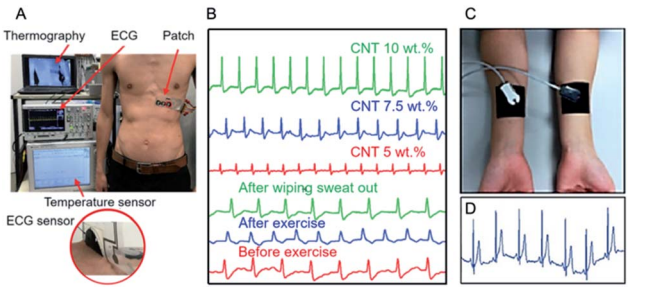

Fig. 10 (A) Photograph of a real-time wearable demonstration with close on ECG sensors during adhesion test; adapted/reproduced from ref. 153 with permission from American Association for the Advancement of Science, Copyright 2020; (B) real-time ECG signals using different CNT concentrations and before and after exercise; adapted/reproduced from ref. 154 with permission from Wiley, Copyright 2020; (C) photograph of MWCNT–PDMS electrode; (D) ECG signal for MWCNT–graphene/PDMS electrode during motion; adapted from ref. 155 with permission from American Chemical Society, Copyright 2020.

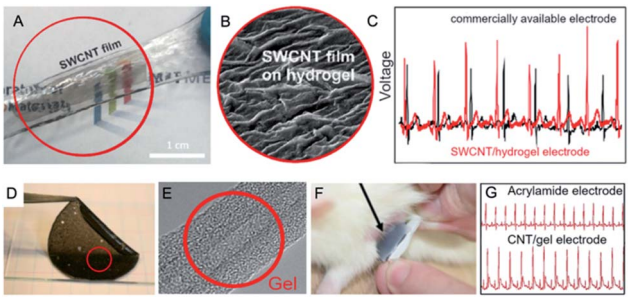

Fig. 11 (A) Photograph and SEM micrograph (B) of SWCNT/hydrogel structure at the stretched state; (C) ECG signal for SWCNT/hydrogel electrode compared to Ag/AgCl electrode; figures have been adapted/reproduced from ref. 126 with permission from American Chemical Society, Copyright 2020; (D) photograph of a sheet of conductive gel for ECG electrode; (E) TEM image of CNT–gel hybrid Copyrights Nature Publishing Group; (F) placing the ECG electrode on the rat skin; (G) ECG signals for acrylamide electrode and CNT/gel electrode; figures have been reproduced/adapted from ref. 135 with permission from Nature Publishing Group, Copyright 2020.

electric circuit transmitting signals to outer devices, while PDMS protected and insulated the lower layers. Impedance of the electrode was MWCNT concentration-dependent, and even if it was of an order of magnitude higher than for the standard electrode, the ECG signal was time-stable and its quality was similar to the latter (Fig. 9A and B). It is worthy of note that no difference in ECG-waveform was observed during multiple peel-offs. In a similar but less comprehensive approach, Tripathi *et al.*[152] fabricated electrodes using CNTs and two types of PDMS: adhesive and non-adhesive. The electrode included four layers: aPDMS, CNTs dispersed in aPDMS, polyamide doped with silver and titanium and non-adhesive PDMS layer. ECG signals were again comparable to the conventional electrode.

Kang *et al.*[136] demonstrated wearable SWCNT-based dry-electrodes (d = 1.2–2 nm, l = 5 μm). This solution could be competitive to the wet standard Ag/AgCl electrodes. A metal snap was immersed in PDMS solution – deposited by drop-casting – on a glass substrate and the system was cured in vacuum. Subsequently, PDMS mould was detached and the SWCNT paste was dropped onto the PDMS mould. A metal snap could be straightforwardly connected to the conventional ECG cable with a clip. The electrode of contact resistance *ca.* 10 Ω sq^{-1} acquired ECG wave-form regardless of the patient's sweat and motion. The electrode was not compatibilized with any textile, but it was an element of wearable electronics.

An analogous method for electrode fabrication was presented by Chi *et al.*[137] who studied the effect of MWCNT concentration on the quality of ECG signal recorded using the MWCNT/PDMS electrodes (Fig. 9C). And so, when MWCNT (d = 8–15 nm, l = 50 μm) concentration was higher than 5.5 wt%, the impedance was lower than for standard electrode, while for concentration lower than 4 wt%, the ECG signal had a smaller amplitude and high motion artefacts were observed. Indeed, for concentration in the range of 4–8 wt% no significant differences between signal quality was observed. On the other hand, the baseline for the standard Ag/AgCl electrode was more sensitive to motion. After two days gel dried off and, hence ECG signal for Ag/AgCl electrode was reduced. Contrarily, for MWCNT/PDMS electrode no changes in the ECG signals recording were observed for 7 days. Yamamoto *et al.*[132] prepared ECG electrode based on MWCNTs (10 wt%) and PDMS but using ethoxylated polyethylenimine (PEIE) as the adhesion enhancer. The electrode could be used at least for hundred attachment cycles and under sweat conditions without any changes in the ECG signal. Furthermore, the composite did not cause any skin irritation during a 30 h-test (Fig. 9D). Critically, the electrode enabled recording ECG signals during rest, standing and sitting, and walking/running (Fig. 9E).

In 2016 Yamamoto *et al.*[153] presented printable flexible device which could be used as a skin temperature sensor, an ECG sensor, environmental ultraviolet sensor and motion sensor (Fig. 10A) – with Ag electrodes as the key elements whereas CNTs were used as thin-film transistors and elements of strain and temperature sensors. The complex system though suffered from a low-amplitude ECG signal which was assigned to the insulating adhesive layer between skin and the sensor. In the follow-up work[154] this problem was solved using MWCNTs and PEIE compatibilizer and therefore enhancer of PDMS adhesivity. The electrode could register medical quality of ECG signal for at least 100 attaching–detaching cycles even if its impedance was eight times higher than for the standard electrode (Fig. 10B). On the other hand, prolonged storing in air negatively affected the electrode performance. Kim *et al.*[155] proposed hierarchical, elastomeric nanocomposite as the ECG electrode material. The structure contained 1 wt% of MWCNTs (d = 10 nm, l = 10 μm) and graphene flakes (lateral size 4.5 μm, flake thickness 12 nm) (9 : 1) dispersed in PDMS matrix. The simultaneous incorporation of MWCNTs and graphene into the elastomeric matrix had a synergic effect toward crossing the percolation threshold. The minor amount of broader and flat graphene flakes played a key role as activators reviving the partially electrically inactive regions where the conductive paths were disrupted, hence it helped to reduce the volume resistivity of the composite. High flexibility and excellent adhesion were provided by silicon microparticles with mushroom-shaped holes. The ECG signal had a high amplitude and a well-

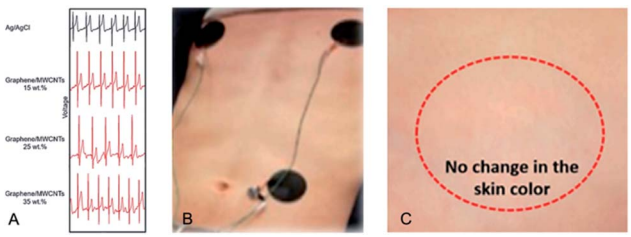

Fig. 12 (A) The chest ECG signals recorded by the different types of electrodes: conventional Ag/AgCl, graphene/MWCNTs-15%, graphene/MWCNTs-25%, and graphene/MWCNTs-35%; (B) photograph of graphene/MWCNT electrodes and (C) the skin-compatibility test of the electrode; figures have been adapted/reproduced from ref. 134 with permission from Multidisciplinary Digital Publishing Institute, Copyright 2020.

established baseline; however, a lot of noises was observed upon patient's motions (Fig. 10D).

Interestingly, the electrode collected signals (though of low amplitude) even under water due to the water-repellent characteristics. Martinez *et al.*[139] prepared electrodes for recording ECG by immobilization of MWCNTs ($d = 70$ nm, $l = 120$ μm) on poly(vinylidene fluoride) (PVDF) filters using poly(*N*-vinylpyrrolidone) (PVP-40) as MWCNT dispersant (1 g PVP-40 per 100 mg MWCNTs in 20 mL of water). MWCNT dispersions were filtered off through PVDF filters and dried. Electrical resistance of the electrode was over hundred times higher than for Ag conductive paint, however at hundred times lower weight. The MWCNT/PVDF electrode was able to record ECG signals with high sensibility, similar resolution and slightly noisier baseline as compared to the neat Ag electrode.

Demonstrating development in the field, Gilshteyn *et al.*[126] prepared electrically conductive hydrogels as skin-like electrodes for wearable electronics (Fig. 11A and B).

The 40 nm-thick SWCNT film on a nitrocellulose filter was pressed against the hydrogel prepared by reacting alginate and acrylamide with cross-linkers (*N*,*N*-methylenebis(acrylamide), $CaSO_4$, cross-linking accelerator (*N*,*N*,*N*′,*N*′-tetramethylethylenediamine) and initiator $(NH_4)_2S_2O_8$) under UV-curing (254 nm, 8 W, 1 h). The filter could be simply peeled off leaving the SWCNT film on the hydrogel surface of electrical resistance between 200 Ω and 28 kΩ – depending on stretching/releasing cycle. The sheet resistance of the SWCNT/hydrogel structure was 100 Ω sq^{-1}. The electrode could measure the ECG signal (Fig. 11C) of higher amplitude and enhanced signal-to-noise ratio as compared to the standard electrode. Although the proposed solution could be competitive for glued Ag/AgCl electrode, it cannot be applied as a smart textile component.

Sekitani *et al.*[135] presented biocompatible highly conductive gel composite (Fig. 11D). The active element was MWCNT sheet ($d = 5$ nm, $l > 100$ μm, sheet thickness 50–150 μm). The matrix was polyrotaxane aqueous gel with a photo-cross-linking agent (irgacure 259). The gel composite had high AC admittance of 100 mS cm^{-2}. The gel composite (size: 1 cm^2, thickness 1 mm) of homogenous nanotube coverage (Fig. 11E) was placed on the rat heart for heart signals monitoring (Fig. 11F) and showed a minor skin irritation reaction compared with the metallic electrodes. As the reference, commercially available conductive gel comprising a graphite-sheet electrode with acrylamide gel was used. For both types of electrode, ECG signals were clearly visible (Fig. 11G), however, for CNT–gel electrode signal amplitude was much higher. Furthermore, composites successfully monitored ischaemia-induced myocardial infarction on a living heart.

It should be here highlighted that for the polymer electrodes the most promising solution was presented by Peng *et al.*[123] Although similarly to other scientists they used PDMS as the matrix and MWCNTs as the conductive filler, they studied not only electrode composition but also the macro-scale morphology of the nanocomposite. By using the micropillar contacts, they minimized the electrode-skin resistance and, as the consequence, it was possible to acquire ECG signals over long-term periods of patient's movement of comparable quality as for the standard ECG electrodes.

5.2 Textile and paper electrodes

Textile and paper electrodes share some morphological features, mechanical characteristics and processing regimes, and are nowadays considered as versatile and/or greener prospective solutions for textronics and 'flextronics' (flexible electronics). Hossain *et al.*[134] developed a flexible, paper-based electrode with chemically-modified graphene and MWCNTs (oxidised) ($d = 7$–80 nm, $l = 0.5$–2 μm) as fillers. This allowed achieving a uniform dispersion of MWCNTs since graphene acted as a dispersant/stabilizer for MWCNTs. The electrode was prepared by vacuum filtration of graphene/MWCNTs dispersion in *N*,*N*-dimethylformamide by a nylon membrane. The tested nanofiller concentration was 15, 25 and 35 wt% with the highest once enabling decrease of impedance from 60 kΩ (15 wt%) to 30 kΩ (35 wt%) whereas those values were still higher than for Ag/AgCl electrode. The ECG signals were almost the same as those for Ag/AgCl electrode (Fig. 12A). Moreover, changes in the signal amplitude were less significant than for the standard electrode. Last but not the least, the electrodes (Fig. 12B) could be used for long-term monitoring and did not cause any irritation or skin problems (Fig. 12C).

Currently, there is an increasing demand for wearable fitness trackers, smart watches and waist or chest belts for the pulse measurement. Those products although have an extremely low accuracy.[156] This characteristic could not be an essential problem, unless they would be used only by healthy people for the workout control (energy consumption, walked distance, *etc.*). One might nevertheless imagine what could happen if treated, suffering from cardiac diseases or symptoms persons use it for heart monitoring. Obviously, data obtained for 12-lead system is incomparable with that obtained from a two-point belt or wristband electrodes. A solution for those problems could be delivered by textronics and ECG system implemented to (T-)shirts or other clothing. A shirt – in contrast to belts or wristbands – can provide a higher number of points for signal acquisition. Moreover, by the appropriate preparation of

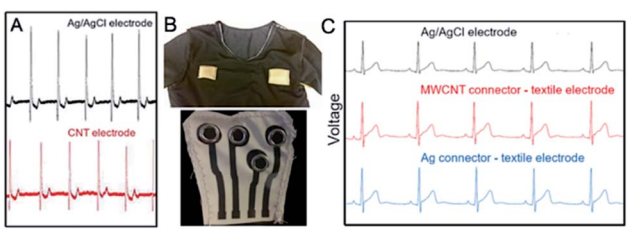

Fig. 13 (A) ECG signal for MWCNT textile electrode *versus* Ag/AgCl electrode; this figure has been adapted from ref. 157 with permission from Multidisciplinary Digital Publishing Institute, Copyright 2020; (B) Textile MWCNT/PU connectors printed on T-shirt; (C) ECG recordings obtained with the three setups: Ag/AgCl electrode (black), MWCNT connector – textile electrode (red) and Ag connector – textile electrode (blue);[147] these figures have been adapted from ref. 147 with permission from Multidisciplinary Digital Publishing Institute, Copyright 2020.

electrode, it could be as comfortable as a typical shirt. Here, a few key solutions should be recalled and discussed.

Kumar *et al.*[133] produced textile electrode using acrylic paint loaded with *O*-MWCNTs ($d = 20$–30 nm, 1 : 1). ECG signals were registered for different electrode dimensions. The highest signal quality was achieved for the 4 cm × 4 cm electrode. These results were in a decent correlation with the results for MWCNT–PDMS electrodes. The signal was also measured for the composite with 2 : 1 (v/v) MWCNT to acrylic paint. However, increasing conductivity of the electrode by increasing the MWCNT volume fraction resulted also in the increased noise sensitivity. Overall, acrylic electrode displayed similar advantages to the PDMS electrode like flexibility, elasticity, and biocompatibility. However, acrylic-based composites/coatings are promising candidates for large-scale smart textiles due to their better adaptability to screen printing.

Further, Jung *et al.*[157] used textile acrylic paint as a matrix for MWCNTs (3 wt%). Printed on the fabric and conditioning yielded the electrode of impedance higher than for Ag/AgCl electrode what resulted in acquiring ECG signal of lower amplitude (Fig. 13A). Nevertheless, the conductive paint allowed for application onto various textiles and after the final refining this method could be very perspective material for wearable electrodes.

Seoane *et al.*[147] used MWCNT ($d = 10$–30 nm, $l = 10$–30 μm)/PU paste to produce interconnectors (conductive paths) between textile electrodes and the electronic instrumentation (Fig. 13B). As a reference, dried silver paste was used. The surface resistivity of MWCNT/PU-coated polyester was 350 Ω sq^{-1} and it changed upon elongation. The interconnectors based on MWCNT/PU paste allowed for recording almost identical signals as Ag-connectors. The results were the equivalent as for Ag/AgCl electrode with a difference that for MWCNT/PU interconnectors signal amplitude was higher (Fig. 13C).

As can be seen from the above analysis, textile solutions are at the beginning of their implementation schemes, but at the constantly growing technological readiness levels. From a purely medical point-of-view, textile electrodes perform better than the polymer glued electrodes. At the moment, the most promising results belong to Seoane *et al.*[147] Their protocol covered *ad hoc* manufactured PU paste of very low electrical resistivity and allowed for recording signals with significantly higher amplitude than for the regular Ag/AgCl electrode.

5.3 Yarn- and fiber-based electrodes

Due to straightforward adaptability to existing technologies and scalability, yarn- and fiber-based electrodes are also expected to be competitive in the production of reliable flexible electrodes. Adhikari *et al.*[142] used electrically conductive fibres (ECF) for the ECG electrode preparation (Fig. 14A and B). Cotton, silk or polyester fibres were dip-coated with conductive ink. The conductive filler was SWCNTs (0.8 mg mL^{-1} in $CHCl_3$), whereas poly(3-hexylthiophene) ($M_n = 10.7$ kDa, PDI = 1.9) served as the electroconductive matrix. The electrical resistance of fibres depended on the number of dippings and did not change after ten dippings (0.5 kΩ cm^{-1} for cotton, 0.65 kΩ cm^{-1} for polyester and 0.73 kΩ cm^{-1} for silk). Those fibres recorded ECG signals (Fig. 14C) with a similar amplitude and signal-to-noise ratio as compared to the standard metallic electrodes. However, the baseline should be improved. It could be achieved by resistance reduction by iodine doping of fibres.

Zhao *et al.*[146] prepared a conductive fabric using SWCNT ($d = 1$–2 nm, $l = 5$–30 μm) coated cotton yarns (CYs) by dip-coating. SWCNT concentration in the aqueous dispersion was 2–16 mg mL^{-1}. CYs were dipped into the dispersion and dried on air for 24 h. The final weight was 8–20% higher than for pristine CY. The fabric combined flexibility of the cotton with high conductivity of SWCNTs. Here, SWCNT-CYs did not serve as an electrode, but replaced the original lead wires (Fig. 14D). ECG signals transferred with SWCNT wires had similar amplitude as the standard wiring; however, the ECG features were found of

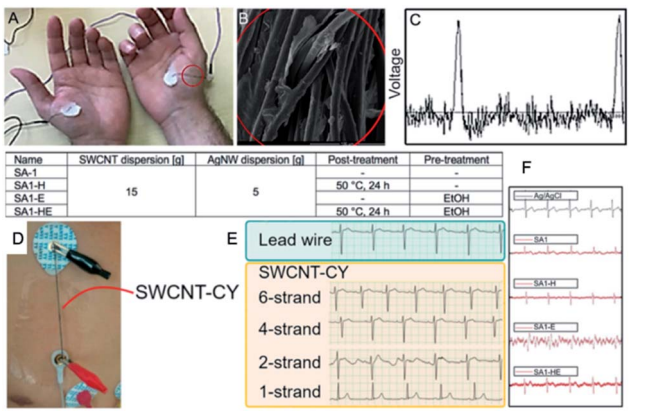

Fig. 14 (A) Photograph of PET-ECF electrode; (B) SEM image of ECFs; (C) ECG recording across left and right thenar muscles using stained polyester ECF; these figures have been adapted/reproduced from ref. 142 with permission from American Chemical Society, Copyright 2020; (D) the photograph of a setup recording and transmitting human ECG signals using the SWNT-cotton yarns; (E) ECG signals using commercial lead wires (light blue area) and SWNT-cotton yarns (light yellow area);[146] these figures have been adapted/reproduced from ref. 146 with permission from Multidisciplinary Digital Publishing Institute, Copyright 2020; (F) comparison of ECG signals in morphology of waveforms for different condition of SWCNT-Ag/PU electrode preparation; this figure has been adapted/reproduced from ref. 145 with permission from IOP Publishing, Copyright 2020.

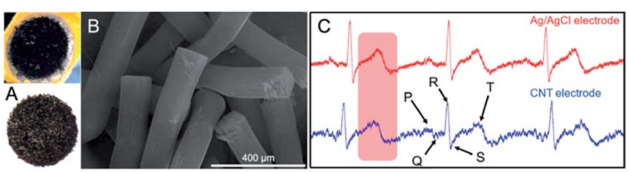

Fig. 15 (A) Photographs and (B) SEM micrograph of ECG electrode based on MWCNT forest; these figures have been reproduced from ref. 140 with permission from IEEE, Copyright 2020; (C) the ECG signal collected by two electrodes for comparison with Ag/AgCl electrode and polypyrrole-coated MWCNT 'forest' electrode; this figure has been adapted from ref. 141 with permission from Multidisciplinary Digital Publishing Institute, Copyright 2020.

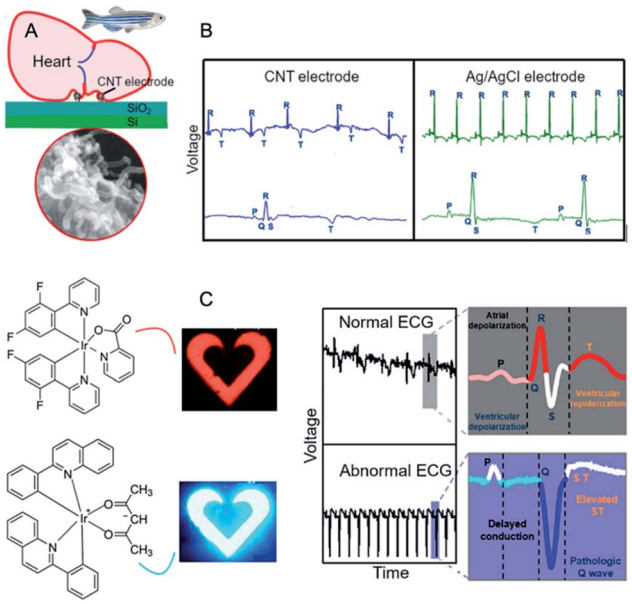

Fig. 16 (A) The schematic of the cardiac recording system for zebrafish using MWCNT-based multilayer microelectrode with its corresponding SEM image; (B) ECG signals for MWCNT microelectrode and Ag/AgCl electrode; these figures have been adapted/reproduced from ref. 143 with permission from Elsevier, Copyright 2020; (C) real-time colour changes of the OLEDs synchronized with the ECG signal; this figure has been adapted/reproduced from ref. 158 with permission from American Chemical Society, Copyright 2020.

Fig. 17 The most important challenges for ECG materials in the light of the implementation routes.

lower amplitude and covered by noise (Fig. 14E). The conductance of a single-strand SWCNT-CY was higher than 4 μS cm^{-1}, thus ECG signal measured by a single-strand SWNT-CY was incorrect.

The same signal measured by the two-strand SWCNT-CYs showed some turbulence and noise. Eventually, the ECG-waveforms measured by four-strand and six-strand SWCNT-CYs were similar to those measured by the lead wires. Nevertheless, washability and long-term stability of such wires remain a challenge.

Changing the pristine fibre material, Lee *et al.*[145] fabricated wearable textile ECG sensors with polyurethane nanoweb was dip-coated using 1 wt% aqueous dispersion of SWCNTs (d = 1.1–1.7 nm, l = 5–30 μm) and Ag nanowires (d = 30–35 nm, l = 20–25 μm). The researchers studied the effect of pre-treatment (dipping in ethanol) and post-treatment (heating at 50 °C for 24 h) on the ECG signal (Fig. 14F). The signal emerged of high intensity and stable regardless of motion, age, sex and body mass index of the patients. However, it was not medically reliable due to the placement of electrodes (the inner forearm). The signal waveforms measured by all textile electrodes showed P-waves, QRS-complex, as well as T- and U-waves. Particularly, the waveforms of electrode SA1-H (without pre-treatment, post-treated) showed the most similarity to those of the Ag/AgCl electrode, and consistently stable signal quality. It was the consequence of the lowest linear resistance and contact impedance for SA1-H electrode. Moreover, SA1-H electrode had higher tensile strength and elongation at break than the untreated.

Although of promising functionalities, all of the above yarn- and fiber-based electrodes are nonetheless characterized by the same unknown factor possibly transposed to the significant shortcoming, *i.e.* the lack of washability test. If those solutions are to be used as electrodes, they cannot change their characteristics for at least five washings under standardized conditions. Hence, if any of those solutions fulfils the requirements from the washing resistance tests, any shape of the electroconductive path would be achievable, and what is of the great importance – accompanied by the full textile-to-paint physicochemical compatibility.

5.4 Free-standing/pure CNT materials

Application of free-standing – vertically/horizontally aligned or isotropic – CNT arrays emerges as the most instant at the first glance. And although mechanical stability of such systems does not guarantee time-stable ECG signals especially under movement conditions, this direct approach was also verified experimentally. And so, Abu-Saude *et al.*[140] prepared a self-standing electrode from vertically aligned MWCNT 'forest' (d = 10–30 nm, length/thickness 1–1.5 mm) (Fig. 15A and B). As the substrate for the MWCNT growth in catalytic chemical vapour deposition (c-CVD), circular 10 mm-stainless steel foil covered with Al_2O_3 (10 nm) and iron (1–2 nm) was used. Although the MWCNT electrode was capable of capturing ECG signals, the research was preliminary. Nevertheless, the introductory research was continued[141] and the problem with the poor adhesivity of the MWCNT electrode to the substrate was solved by coating of CNTs with polypyrrole (PPy). This operation allowed recording ECG signals with a similar resolution as for

the Ag/AgCl electrode – indeed, the QRS-complex could be clearly visible on the electrocardiogram (Fig. 15C).

Shih *et al.*[143] applied nanotube microelectrode array for ECG study in an animal model, *i.e.* adult zebrafish (Fig. 16A). *O*-MWCNT-based electrodes were used not only for ECG signal recording but also for drug-screening. 3D microelectrode was prepared by combination of plasma-enhanced CVD, spin-coating and photolithography. And so, on the multilayer structure of Si wafer, SiO_2, Ti, Ni and Au, MWCNTs ($d = 20$ nm, $l = 1.5$–3.9 μm) were synthesised at 400 °C from C_2H_2.[144] The electrode was able to detect ECG signal of excellent quality (Fig. 16B). As compared to Ag/AgCl electrode the signal amplitude was however lower due to lower impedance. On the other hand, it should be pointed that the standard Ag/AgCl electrode was thousand times larger than the 3D microelectrode. In fact, the 3D-CNT micro-electrode array was also able to detect the ECG signals at various anatomical regions of the isolated zebrafish heart.

Koo *et al.*[158] designed wearable ECG monitor based on CNTs integrated with voltage-dependent colour-tunable OLEDs. The ECG signals were measured by thin serpentine-shaped gold film as the electrode. Semiconducting CNTs modified with metal-oxide acted as an amplifier. The ECG signals were sixty times stronger using the amplifier as compared to the non-amplified signals. After processing, the signal was visualized by OLEDs – red for normal cardiac signal and blue for abnormal cardiac signal (Fig. 16C). The colour tuning was the result of placing exciton-blocking layer of bis[2-(diphenylphosphino)phenyl]-ether oxide between two emitting layers for blue (bis[2-(4,6-difluorophenyl)pyridinato-C2,*N*](picolinato)-iridium(III)) and for red (bis(2-phenylquinolyl-*N*,C(2′))-iridium(acetylacetonate)) dyes.

The above-discussed solutions principally belong to purely scientific propositions. Although the solution presented by Koo *et al.*[158] might pave novel pathways, still CNTs were used there only rather as a signal amplifier. In fact, all of the elaborated free-standing electrodes bring some novelty to the field, however, due to poor reproducibility, diminished performance over time, complex manufacture, and unsatisfactory economy, they cannot be expected in the forthcoming future as of good prognostics for the massive technological transfers.

6. Conclusions and perspectives

There is a clear interest in the development of novel ECG sensors at this time. An increasing number of prototypes of glued electrodes as well as textile sensors is continuously emerging. But still, there is a large deficit in the faultless systems which could compete with the conventional ECG Holter method. All solutions so-far provided ECG signal of nearly or fully medical quality, but in the same time, all of them required amplification. Many of the solutions were founded on metallic conductors in a variety of functions – from electrodes to contacts to wiring – which although provide high conductivity, but also significantly increase weight, sensitivity to corrosion, and decreased biocompatibility. Additionally, even adhesive sensors of higher performance did not provide stable signals during the motion. Their long-time use frequently leads to attenuation of signals and reduced quality of the baseline.

Based on the analysis, one might specify the most important challenges in this field (Fig. 17). In order to achieve ECG signals of high amplitude and stability, noiseless and with the stable baseline one could employ only-CNT materials of excellent electroconductivity.

This is currently possible but economically more justified would be manufacturing composites containing ultra-long CNT fillers, admixed with additives and other conductive carbon nanoallotropes – only as long as the overall and rigorous criteria containing mechanics (*e.g.* light weight, comfort, adhesion providing stable signals deriving from low skin-electrode impedance, lack of motion artefacts), biosafety, washability, and recyclability – to name the most important ones – are fulfilled. Another challenge is uniformity of the electrodes to avoid differences between impedance. Comfortability and light weight are obviously particularly for bedridden patients and patients requiring long-time monitoring. One might claim that the most prospective solution in the nearest time horizon is the incorporation of high-performance electrodes into clothes. This unification shall connect the advantages of metallic conductors with comfort and processability of textiles in the broadest context, *i.e.* from designing the precursor, the actual fibre production and processing to textile manufacture with the relevant modifications and workup.

Conflicts of interest

There are no conflicts to declare.

Acknowledgements

The authors greatly acknowledge National Science Centre in Poland for financing the research in the framework of the OPUS program 2019/33/B/ST5/01412.

Notes and references

1 S. Iijima, *Nature*, 1991, **354**, 56–58.
2 X. Jia and F. Wei, *Top. Curr. Chem.*, 2017, **375**, 18.
3 M. H. Moaieri, A. Rahi, F. Sharifi and K. Navi, *J. Appl. Res. Technol.*, 2017, **15**, 233–241.
4 S. Joshi, V. D. Bhatt, E. Jaworska, A. Michalska, K. Maksymiuk, M. Becherer, A. Gagliardi and P. Lugli, *Sci. Rep.*, 2018, **8**, 11386.
5 G. Hills, C. Lau, A. Wright, S. Fuller, M. D. Bishop, T. Srimani, P. Kanhaiya, R. Ho, A. Amer, Y. Stein, D. Murphy, Arvind, A. Chandrakasan and M. M. Shulaker, *Nature*, 2019, **572**, 595–602.
6 A. Kolanowska, D. Janas, A. P. Herman, R. G. Jedrysiak, T. Gizewski and S. Boncel, *Carbon*, 2018, **126**, 31–52.
7 J. G. Wang, H. Liu, X. Zhang, X. Li, X. Liu and F. Kang, *Small*, 2018, **14**, 1703950.
8 T. Lv, Y. Yao, N. Li and T. Chen, *Nanotoday*, 2016, **11**, 644–660.

9 S. Boncel, A. Zniszczol, M. Pawlyta, K. Labisz and G. Dzido, *Heat Mass Transfer*, 2018, **54**, 333–339.
10 R. Beigmoradi, A. Samimi and D. Mohebbi-Kalhori, *Beilstein J. Nanotechnol.*, 2018, **9**, 415–435.
11 N. Muralidharan, E. Teblum, A. S. Westover, D. Schauben, A. Itzhak, M. Muallem, G. D. Nessim and C. L. Pint, *Sci. Rep.*, 2018, **8**, 17662.
12 A. Kolanowska, A. W. Kuziel, A. P. Herman, R. G. Jedrysiak, T. Gizewski and S. Boncel, *Prog. Org. Coat.*, 2019, **130**, 260–269.
13 L. Vertuccio, L. Guadagno, G. Spinelli, P. Lamberti, M. Zarrelli, S. Russo and G. Iannuzzo, *Composites, Part B*, 2018, **147**, 42–46.
14 J. Hirotani and Y. Ohno, *Top. Curr. Chem.*, 2019, **377**, 3.
15 Z. Li, A. L. B. de Barros, D. C. Ferreira Soares, S. N. Moss and L. Alisaraie, *Int. J. Pharm.*, 2017, **524**, 41–54.
16 N. Jumar Mehra and S. Palakurthi, *Drug Discovery Today*, 2016, **21**, 585–597.
17 S. Boncel, A. Pluta, M. Skonieczna, A. Gondela, B. Maciejewska, A. P. Herman, R. G. Jedrysiak, S. Budniok, K. Komedera, A. Blachowski and K. Z. Walczak, *J. Nanomater.*, 2017, **2017**, 1–13.
18 R. Prasad and B. R. Bhat, *Sens. Actuators, B*, 2015, **220**, 81–90.
19 S. Han, W. Liu, M. Zheng and R. Wang, *Anal. Chem.*, 2020, **92**, 4780–4787.
20 N. Anzar, R. Hasan, M. Tyagi, N. Yadav and J. Narang, *Sensors International*, 2020, **1**, 100003.
21 S. Park, M. Vosguerichian and Z. Bao, *Nanoscale*, 2013, **5**, 1727–1752.
22 A. Venkataraman, E. V. Amadi, Y. Chen and C. Papadopoulos, *Nanoscale Res. Lett.*, 2019, **14**, 220.
23 H. He, L. A. Pham-Huy, P. Dramou, D. Xiao, P. Zuo and C. Pham-Huy, *BioMed Res. Int.*, 2013, **2013**, 578290.
24 G. A. Mensah, G. S. Wei, P. D. Sorlie, L. J. Fine, Y. Rosenberg, P. G. Kaufmann, M. E. Mussolino, L. L. Hsu, E. Addou, M. M. Engelgau and D. Gordon, *Circ. Res.*, 2017, **120**, 366–380.
25 D. Mozaffarian, *J. Am. Coll. Cardiol.*, 2014, **64**, 1307–1309.
26 L. M. Hurxthal, *N. Engl. J. Med.*, 1934, **211**, 431–437.
27 I. Sim, *N. Engl. J. Med.*, 2019, **381**, 956–968.
28 M. Loukas, P. Youssef, J. S. Gielecki, J. A. Walocha, K. Natsis and R. S. Tubbs, *Clin. Anat.*, 2016, **29**, 270–284.
29 P. J. Hunter, A. J. Pullan and B. H. Smaill, *Annu. Rev. Biomed. Eng.*, 2003, **5**, 147–177.
30 M. Kumar Das and D. P. Zipes, *Electrocardiography of Arrhythmias: A Comprehensive Review: A Companion to Cardiac Electrophysiology*, Elsevier Health Sciences, 2012.
31 J. W. Hurst, *Circulation*, 1998, **98**, 1937–1942.
32 B. Colbert, J. Ankney, J. Wilson and J. Havrilla, *An Integrated Approach to Health Sciences: Anatomy and Physiology, Math, Chemistry and Medical Microbiology*, Cengage Learning, 2011.
33 G. D. Gargiulo, P. Bifulco, M. Cesarelli, A. L. McEwan, H. Moeinzadeh, A. O'Loughlin, I. M. Shugman, J. C. Tapson and A. Thiagalingam, *Sensors*, 2018, **18**, 2353.
34 B. Liu, Z. Luo, W. Zhang, Q. Tu and X. Jin, *Sens. Actuators, A*, 2016, **247**, 459–464.
35 P. J. Xu, H. Zhang and X. M. Tao, *Text. Prog.*, 2008, **40**, 183–213.
36 T. Tamura and W. Chen, *Seamless Healthcare Monitoring: Advancements in Wearable, Attachable and Invisible Devices*, Springer, 2017.
37 S. Suave Lobodzinski and M. M. Laks, *Cardiol. J.*, 2008, **15**, 477–480.
38 E. Ghavanloo and S. A. Fazelzadeh, *Meccanica*, 2016, **51**, 41–54.
39 N. Grobert, *Mater. Today*, 2007, **10**, 28–35.
40 O. V. Kharissova and B. I. Kharisov, *RSC Adv.*, 2014, **4**, 30807–30815.
41 D. Nakar, G. Gordeev, L. D. Machado, R. Popovitz-Biro, K. Rechav, E. F. Oliveira, P. Kusch, A. Jorio, D. S. Galvao, S. Reich and E. Joselevich, *Nano Lett.*, 2020, **20**, 953–962.
42 A. Venkataraman, E. V. Amadi, Y. Chen and C. Papadopoulos, *Nanoscale Res. Lett.*, 2019, **14**, 220.
43 M. F. Yu, B. S. Files, S. Arepalli and R. S. Ruoff, *Phys. Rev. Lett.*, 2000, **84**, 5552–5555.
44 M. Yu, *Science*, 2000, **287**, 637–640.
45 J. Hone, M. Whitney, C. Piskoti and A. Zettl, *Phys. Rev. B: Condens. Matter Mater. Phys.*, 1999, **59**, R2514–R2516.
46 P. Kim, L. Shi, A. Majumdar and P. L. McEuen, *Phys. Rev. Lett.*, 2001, **87**, 215502.
47 K. B. K. Teo, C. Singh, M. Chhowalla and W. I. Milne, Catalytic synthesis of carbon nanotubes and nanofibers, *Encyclopedia of Nanoscience and Nanotechnology X*, American Scientific Publishers, 2003.
48 T. W. Odom, J. L. Huang, P. Kim and C. M. Lieber, *Nature*, 1998, **391**, 62–64.
49 A. Thess, R. Lee, P. Nikolaev, H. Dai, P. Petit, J. Robert, C. Xu, Y. Hee Lee, S. Gon Kim, A. G. Rinzler, D. T. Colbert, G. E. Scuseria, D. Tomanek, J. E. Fischer and R. E. Smalley, *Science*, 1996, **273**, 483–487.
50 L. Forro and C. Schonenberger, *Carbon Nanotubes*, Springer Berlin Heidelberg, 2007.
51 A. De Heer Walt, *MRS Bull.*, 2004, **29**, 281–285.
52 C. Schonenberger, A. Bachtold, C. Strunk, J. P. Salvetat and L. Forro, *Appl. Phys. A: Mater. Sci. Process.*, 1999, **69**, 283–295.
53 G. Chai and Q. Chen, *J. Compos. Mater.*, 2010, **44**, 2863–2873.
54 C. Subramaniam, T. Yamada, K. Kobashi, A. Sekiguchi, D. N. Futaba, M. Yumura and K. Hata, *Nat. Commun.*, 2013, **4**, 2202.
55 J. W. Mintmire, B. I. Dunlap and C. T. White, *Phys. Rev. Lett.*, 1992, **68**, 631–634.
56 N. Hamada, S. I. Sawada and A. Oshiyama, *Phys. Rev. Lett.*, 1992, **68**, 1579–1581.
57 C. P. S. M. Nogueira and J. G. Guimaraes, *Int. J. Circuits, Syst. Signal Process.*, 2015, **9**, 289–295.
58 T. Ando, *J. Phys. Soc. Jpn.*, 2005, **74**, 777–817.
59 A. H. Castro Neto, F. Guinea, N. M. R. Peres, K. S. Novoselov and A. K. Geim, *Rev. Mod. Phys.*, 2009, **81**, 109–162.

60 P. McEuen, M. Bockrath, D. Cobden, Y. G. Yoon and S. Louie, Disorder, *Phys. Rev. Lett.*, 1999, **83**, 5098–5101.
61 P. R. Wallace, *Phys. Rev.*, 1947, **71**, 622–634.
62 K. Wakabayashi, K. Sasaki, T. Nakanishi and T. Enoki, *Sci. Technol. Adv. Mater.*, 2010, **11**, 054504.
63 V. Gayathri, M. Devarajan, A. Ramasubbu and V. Varadan, *Proc. SPIE*, 2003, **5062**, 56–60.
64 T. W. Odom, *Aust. J. Chem.*, 2001, **54**, 601–604.
65 J. R. Chen, C. I. Weng and S. J. Sun, *J. Appl. Phys.*, 2008, **104**, 114310.
66 A. Bachtold, M. S. Fuhrer and S. Plyasunov, *Phys. Rev. Lett.*, 2000, **84**, 6082–6085.
67 G. Galimberti, S. Ponzoni, A. Cartella, M. T. Cole, S. Hofmann, C. Cepek, G. Ferrini and S. Pagliara, *Carbon*, 2013, **57**, 50–58.
68 H. J. Li, W. G. Lu, J. J. Li, X. D. Bai and C. Z. Gu, *Phys. Rev. Lett.*, 2005, **95**, 1–4.
69 P. R. Bandaru, *J. Nanosci. Nanotechnol.*, 2007, **7**, 1239–1267.
70 Y. Bai, R. Zhang, X. Ye, Z. Zhu, H. Xie, B. Shen, D. Cai, B. Liu, C. Zhang, Z. Jia, S. Zhang, Z. Li and F. Wei, *Nat. Nanotechnol.*, 2018, **13**, 589–595.
71 P. Singh, *Int. Arch. Appl. Sci. Technol.*, 2013, **4**, 55–56.
72 S. Abdalla, F. Al-Marzouki, A. A. Al-Ghamdi and A. Abdel-Daiem, *Nanoscale Res. Lett.*, 2015, **10**, 358.
73 G. Rahman, Z. Najaf, A. Mehmood, S. Bilal, A. Ul Haq Ali Shah, S. A. Mian and G. Ali, *C*, 2019, **5**, 3.
74 M. F. Yu, B. S. Files, S. Arepalli and R. S. Ruoff, *Phys. Rev. Lett.*, 2000, **84**, 5552–5555.
75 N. Saifuddin, A. Z. Raziah and A. R. Junizah, *J. Chem.*, 2013, **2013**, 676815.
76 A. F. G. Pereira, J. V. Fernandes, J. M. Antunes and N. A. Sakharova, *Phys. Status Solidi B*, 2016, **253**, 366–376.
77 A. Ghavamian, M. Rahmandoust and A. Ochsner, *Composites, Part B*, 2013, **44**, 52–59.
78 N. Hu, K. Nunoya, D. Pan, T. Okabe and H. Fukunaga, *Int. J. Solids Struct.*, 2007, **44**, 6535–6550.
79 P. A. Gowri Sankar and K. Udhaya Kumar, *Eur. J. Sci. Res.*, 2011, **60**, 342–358.
80 S. Yamashita, Y. Saito and J. H. Cho, *Carbon Nanotube and Graphene Photonics*, Woodhead Publishing, Oxford, 2013, pp. 3–25.
81 J.-C. Charlier, X. Blasé and S. Roche, *Rev. Mod. Phys.*, 2007, **79**, 677–732.
82 K. Gharbavi and H. Badehian, *AIP Adv.*, 2015, **5**, 077155.
83 R. B. Weisman and S. M. Bachilo, *Nano Lett.*, 2003, **3**, 1235–1238.
84 E. Malic, M. Hirtschultz, F. Milde, A. Knorr and S. Reich, *Phys. Rev. B: Condens. Matter Mater. Phys.*, 2006, **74**, 195431.
85 K. Mizuno, J. Ishii, H. Kishida, Y. Hayamizu, S. Yasuda, D. N. Futaba, M. Yumura and K. Hata, *Proc. Natl. Acad. Sci. U. S. A.*, 2009, **106**, 6044–6047.
86 M. Mir, E. Ebrahimnia-Bajestan, H. Niazmand and M. Mir, *Comput. Mater. Sci.*, 2012, **63**, 52–57.
87 K. Saaskilahti, J. Oksanen, S. Volz and J. Tulkki, *Phys. Rev. B: Condens. Matter Mater. Phys.*, 2015, **91**, 115426.
88 J. Wang and J.-S. Wang, *Appl. Phys. Lett.*, 2006, **88**, 111909.
89 H. Das, *Res. Rev.: J. Mater. Sci.*, 2017, **5**, 10–15.
90 Z. Han and A. Fina, *Prog. Polym. Sci.*, 2011, **36**, 914–944.
91 B. Kumanek and D. Janas, *J. Mater. Sci.*, 2019, **54**, 7397–7427.
92 M. E. Itkins, F. Borondics, A. Yu and R. C. Haddon, *Nano Lett.*, 2007, **7**, 900–904.
93 G. H. Xu, Q. Zhang, J. Q. Huang, M. Q. Zhao, W. P. Zhou and F. Wei, *Langmuir*, 2010, **26**, 2798–2804.
94 S. Kim, J. Yim, X. Wang, D. D. C. Bradley, S. Lee and J. C. DeMello, *Adv. Funct. Mater.*, 2010, **20**, 2310–2316.
95 A. Schindler, J. Brill, N. Fruehauf, J. P. Novak and Z. Yaniv, *Phys. E*, 2007, **37**, 119–123.
96 Y. Murakami, S. Chiashi, Y. Miyauchi, M. Hu, M. Ogura, T. Okubo and S. Maruyama, *Chem. Phys. Lett.*, 2004, **385**, 298–303.
97 N. Bahabtu, C. C. Young, D. E. Tsentalovich, O. Kleinerman, X. Wang, A. W. K. Ma, E. A. Bengio, R. F. Ter Waarbeek, J. J. De Jong, R. E. Hoogerwerf, S. B. Fairchild, J. B. Ferguson, B. Maruyama, J. Kono, Y. Talmon, Y. Cohen, M. J. Otto and M. Pasquali, *Science*, 2013, **339**, 182–186.
98 X. He, W. Gao, L. Xie, B. Li, Q. Zhang, S. Lei, J. M. Robinson, E. H. Haroz, S. K. Doorn, W. Wang, R. Vajtai, P. M. Ajayan, W. Wade Adams, R. H. Hauge and J. Kono, *Nat. Nanotechnol.*, 2016, **11**, 633–638.
99 Y. L. Li, *Science*, 2004, **304**, 276–278.
100 C. Paukner and K. K. K. Koziol, *Sci. Rep.*, 2015, **4**, 3903.
101 A. Kolanowska, A. W. Kuziel, R. G. Jedrysiak, M. Krzywiecki, E. Korczeniewski, M. Wisniewski, A. P. Terzyk and S. Boncel, *Nanomaterials*, 2019, **9**, 1619.
102 A. Kolanowska, A. Kuziel, Y. Li, S. Jurczyk and S. Boncel, *RSC Adv.*, 2017, **7**, 51374–51381.
103 A. Kolanowska, P. Wasik, W. Zieba, A. P. Terzyk and S. Boncel, *RSC Adv.*, 2019, **9**, 37608–37613.
104 M. S. P. Shaffer and A. H. Windle, *Adv. Mater.*, 1999, **11**, 937–941.
105 F. Du, J. E. Fischer and K. I. Winey, *J. Polym. Sci., Part B: Polym. Phys.*, 2003, **41**, 3333–3338.
106 R. Andrews, D. Jaques, D. Qian and T. Rantell, *Acc. Chem. Res.*, 2002, **35**, 1008–1017.
107 B. Safadi, R. Andrews and E. A. Grulke, *J. Appl. Polym. Sci.*, 2002, **84**, 2660–2669.
108 Y. Dror, W. Salalha, R. L. Khalfin, Y. Cohen, A. L. Yarin and E. Zussman, *Langmuir*, 2003, **19**, 7012–7020.
109 D. E. Hill, Y. Lin, A. M. Rao, L. F. Allard and Y. P. Sun, *Macromolecules*, 2002, **35**, 9466–9471.
110 P. Potschke, A. R. Bhattacharyya and A. Janke, *Eur. Polym. J.*, 2004, **40**, 137–148.
111 J. Y. Kim and S. H. Kim, *J. Polym. Sci., Part B: Polym. Phys.*, 2006, **44**, 1062–1071.
112 R. Haggenmueller, W. Zhou, J. E. Fischer and K. I. Winey, *J. Nanosci. Nanotechnol.*, 2016, **3**, 105–110.
113 D. Qian, E. C. Dickey, R. Andrews and T. Rantell, *Appl. Phys. Lett.*, 2000, **76**, 2868–2870.
114 K. K. K. Koziol, S. Boncel, M. S. P. Shaffer and A. H. Windle, *Compos. Sci. Technol.*, 2011, **71**, 1606–1611.
115 H. Jin Yoo, Y. Chae Jung, N. Gopal Sahoo and J. Whan Cho, *J. Macromol. Sci., Part B: Phys.*, 2006, **45**, 441–451.

116 T. Evgin, H. Dogacan Koca, N. Horny, A. Turgut, I. H. Tavman, M. Chirtoc, M. Omastova and I. Novak, *Composites, Part A*, 2016, **82**, 208–213.
117 V. Kumar, N. Sharma and S. S. Maitra, *Int. Nano Lett.*, 2017, **7**, 243–256.
118 K. Aoki and N. Saito, *Nanomaterials*, 2020, **10**, 264.
119 J. M. Tan, P. Arulselvan, S. Fakurazi, H. Ithnin and M. Z. Hussein, *J. Nanomater.*, 2014, **2014**, 917024.
120 J. Chlopek, B. Czajkowska, B. Szaraniec, E. Frackowiak, K. Szostak and F. Beguin, *Carbon*, 2006, **44**, 1106–1111.
121 B. Liu, Z. Luo, W. Zhang, Q. Tu and X. Jin, *J. Biomater. Sci., Polym. Ed.*, 2016, **27**, 1899–1908.
122 J. H. Lee, Y. W. Nam, H. C. Jung, D. H. Baek, S. H. Lee and J. S. Hong, *BioChip J.*, 2012, **6**, 91–98.
123 H. L. Peng, J. Q. Liu, H. C. Tian, B. Zu, Y. Z. Dong, B. Yang, X. Chen and C. S. Yang, *Sens. Actuators, A*, 2015, **235**, 48–56.
124 B. Liu, H. Tang, Z. Luo, W. Zhang, Q. Tu and Z. Jin, *Sens. Actuators, A*, 2017, **265**, 79–85.
125 J. Jung, S. Shin and Y. T. Kim, *Microelectron. Eng.*, 2019, **203–204**, 25–30.
126 E. P. Gilshteyn, S. Lin, V. A. Kondrashov, D. S. Kopylova, A. P. Tsapenko, A. S. Anisimov, A. John Hart, X. Zhao and A. G. Nasibulin, *ACS Appl. Mater. Interfaces*, 2018, **10**, 28069–28075.
127 A. A. Chlaihawi, B. B. Narakathu, S. Emamian, B. J. Bazuin and M. Z. Atashbar, *Sens. Biosensing Res.*, 2018, **20**, 9–15.
128 A. Kalra, A. Lowe and A. Al-Jumaily, *Biomed. Phys. Eng. Express*, 2019, **5**, 1–18.
129 H. C. Jung, J. H. Moon, D. H. Baek, J. H. Lee, Y. Y. Choi, J. S. Hong and S. H. Lee, *IEEE Trans. Biomed. Eng.*, 2012, **59**, 1472–1479.
130 S. M. Lee, H. J. Byeon, J. H. Lee, D. H. Baek, K. H. Lee, J. S. Hong and S. H. Lee, *Sci. Rep.*, 2014, **4**, 6074.
131 S. M. Lee, J. H. Lee and S. H. Lee, Skin-like electronics based on CNT/PDMS composite for long term and unconscious sensing of biosignals, *IEEE 15th International Conference on Nanotechnology*, Rome, 2015.
132 D. Yamamoto, Y. Yamamoto, M. Takada, H. Naito, T. Arie, S. Akita and K. Takei, *Adhesive Conductive Polymer for Wearable Electrocardiogram Monitoring, International Conference on Solid State Devices and Materials*, Sendai, 2017.
133 P. S. Kumar, P. Rai, S. Oh, H. Kwon and V. K. Varadan, *Nanosystems in Engineering and Medicine*, 2012, p. 8548.
134 M. F. Hossain, J. S. Heo, J. Nelson and I. Kim, *Information*, 2019, **10**, 325.
135 T. Sekitani, T. Yokota, K. Kuribara, M. Kaltenbrunner, T. Fukushima, Y. Inoue, M. Sekino, T. Isoyama, Y. Abe, H. Onodera and T. Someya, *Nat. Commun.*, 2016, **7**, 11425.
136 B. C. Kang and T. J. Ha, *Jpn. J. Appl. Phys.*, 2018, **57**, 05GD02.
137 M. Chi, J. Zhao, Y. Dong and X. Wang, *Materials*, 2019, **971**, 1–11.
138 J. H. Kim, J. Y. Hwang, H. R. Hwang, H. S. Kim, J. H. Lee, J. W. Seo, U. S. Shin and S. H. Lee, *Sci. Rep.*, 2018, **8**, 1375.
139 J. Bernal-Martinez, A. Sesena-Rubfiaro, R. Godinez-Fernandez and A. Aguilar-Elguezabal, *Microelectron. Eng.*, 2016, **166**, 10–14.
140 M. J. Abu-Saude and B. I. Morshed, *IEEE Sens. J.*, 2015, **15**, 5851–5858.
141 M. J. Abu-Saude and B. Morshed, *Chemosensors*, 2018, **6**, 27.
142 S. Adhikari, B. Richter, Z. Mace, R. J. Sclabassi, B. C. Cheng, D. Whiting, S. Averick and T. Nelson, *Ind. Eng. Chem. Res.*, 2018, **57**, 7866–7871.
143 M. Shih, C. T. Kuo, M. H. Lin, Y. J. Chuang, H. Chen and T. R. Yew, *Biocybern. Biomed. Eng.*, 2020, **40**, 701–708.
144 A. I. Pan, M. H. Lin, H. W. Chung, H. Chen, S. R. Yeh, Y. J. Chuang, Y. C. Chang and T. R. Yew, *Analyst*, 2015, **141**, 279–284.
145 E. Lee and G. Cho, *Smart Mater. Struct.*, 2019, **28**, 045004.
146 Y. Zhao, Y. Cao, J. Liu, Z. Zhan, X. Li and W. J. Li, *Micromachines*, 2018, **9**, 132.
147 F. Seoane, A. Soroudi, K. Lu, D. Nilsson, M. Nilsson, F. Abtahi and M. Skrifvars, *Sensors*, 2019, **19**, 4426.
148 J. Y. Baek, J. H. An, J. M. Choi, K. S. Park and S. H. Lee, *Sens. Actuators, A*, 2008, **143**, 423–429.
149 B. Liu, Z. Luo, W. Zhang, Q. Tu and X. Jin, *Sens. Actuators, A*, 2016, **247**, 459–464.
150 B. Liu, Y. Chen, Z. Luo, W. Zhang, Q. Tu and X. Jin, *J. Biomater. Sci., Polym. Ed.*, 2015, **26**, 1229–1235.
151 A. A. Chlaihawi, B. B. Narakathu, S. Emamian, A. Eshkeiti, S. G. A. Reddy, B. J. Bazuin and M. Z. Atashbar, Development of flexible dry ECG electrodes based on MWCNT/PDMS composite, *IEEE Sens. J.*, 2015, 1–4.
152 R. P. Tripathi, A. Tiwari and G. R. Mishra, Design and Fabrication of a Nano Patch Electrode for ECG using CNT/PDMS, *IEEE International Conference on Computing Methodologies and Communication*, Erode, 2017.
153 Y. Yamamoto, S. Harada, D. Yamamoto, W. Honda, T. Arie, S. Akita and K. Takei, *Sci. Adv.*, 2016, **2**, e1601473.
154 Y. Yamamoto, D. Yamamoto, M. Takada, H. Naito, T. Arie, S. Akita and K. Takei, *Adv. Healthc. Mater.*, 2017, **6**, 1700495.
155 T. Kim, J. Park, J. Sohn, D. Cho and S. Jeon, *ACS Nano*, 2016, **10**, 4770–4778.
156 S. C. Mukhopadhyay, H. Ghayvat, J. Liu and X. Gui, *IEEE Sens. J.*, 2015, **15**, 7341–7348.
157 J. Jung, S. Shin, S. Park and Y. T. Kim, Flexible dry electrodes made from CNT/Textile Paint Composite for ECG sensor, *International Conference Biomedical Engineering and Sciences*, Las Vegas, 2016.
158 J. H. Koo, S. Jeong, H. J. Shim, D. Son, J. Kim, D. C. Kim, S. Choi, J. I. Hong and D. H. Kim, *ACS Nano*, 2017, **11**, 10032–10041.